クロスオーバー模型によるQCD相図とクォーク・ハドロン転移へのアプローチ

宮原, 昌久

Approach to QCD phase diagram and quark-hadron transition by a crossover model

Akihisa Miyahara

Theoretical Nuclear Physics, Department of Physics
Graduate School of Science, Kyushu University
744, Motooka, Nishi-ku, Fukuoka 819-0395, Japan

Abstract

Drawing a reliable QCD phase diagram enables to elucidate the origin of matter and the cosmogony and so on. For drawing a QCD phase diagram, the quark-hadron transition is an essential factor. In low density, the quark-hadron transition is crossover. For the crossover, it is difficult to determine the transition temperature clearly. Many authors regarded restoration and breaking of chiral and $\mathbb{Z}_3$ symmetries as indicators of the quark-hadron transition. However, these symmetry breaking and restoration do not stand for the direct transition from the hadron degree of freedom to the quark degree of freedom.

In this thesis, we construct the effective model which has quark and hadron degrees of freedom explicitly. We determine the quark-hadron transition temperature by using the model, and compare the resulting transition temperature with chiral and $\mathbb{Z}_3$ transition temperatures. The comparison shows that chiral and $\mathbb{Z}_3$ transition occur in hadron phase.

Finally, we draw a QCD phase diagram by using our model. At the time, we draw three QCD phase diagrams for baryon number B, isospin number I, hypercharge number Y, respectively. This drawing shows that the quark-hadron transition has the same reaction for changing B, I and Y in low density. We call the phenomenon "BIY approximate equivalence", and discussed the BIY approximate equivalence.

Contents

Chapter 1

Introduction

1.1 Quantum chromodymanics

Quarks and gluons are fundamental particles in nature. They are confined into hadrons by strong interaction. In hadron physics, it is one of the ultimate goals to elucidate the confinement mechanism based on the strong interactions among quarks and gluons.

The Quantum Chromodynamics (QCD) is a remarkable theory of the interaction among quarks and gluons. Its Lagrangian density is defined as

$$\mathcal{L} = \bar{q}(i\gamma_\mu D^\mu - m)q - \frac{1}{4}F^a_{\mu\nu}F^{\mu\nu}_a, \tag{1.1}$$

where q is the quark field, m is the current quark mass matrix and quark fields interact with gluon fields $A_\mu = A^a_\mu \lambda_a/2$ through the covariant derivative $D_\mu = \partial_\mu + igA_\mu$ with the gauge coupling constant g. Here, λ_a $(a = 1, 2, \cdots, 8)$ are the Gell-Mann matrices in color space. The gluon dynamics are governed by the field strength tensor $F^a_{\mu\nu} = \partial_\mu A^a_\nu - \partial_\nu A^a_\mu - g f_{abc} A^b_\mu A^c_\nu$ with the anti-symmetric structure constant f_{abc}.

Quarks are classified with six species called by "flavors": up (u), down (d), strange (s), charm (c), bottom (b), and top (t). c-, b- and t-quark masses are much larger than the typical energy scale of QCD, $\Lambda_{\rm QCD} \sim 200$ MeV. Then these quarks hardly affect low-energy dynamics of our interest. Therefore, we focus on only u, d and s quarks.

From the analysis of the perturbative renormalization group method, QCD has asymptotic freedom. At high energy or at the short distance, quarks behave as non-interactive particles since the coupling constant of QCD becomes small. This asymptotic freedom is characterized by a running (effective) coupling constant of quark-gluon vertex.The coupling constant becomes, in contrast, large at low energy. The coupling constant is described as

$$a(-k^2) \equiv \frac{g^2(k^2)}{4\pi}, \tag{1.2}$$

where

$$g^2(k^2) = \frac{g_\lambda^2}{1 + bg_\lambda^2 \log(-k^2/\Lambda^2)},$$
$$\Lambda^2 = \lambda^2 \exp(-1/bg_\lambda^2),\ b = \left(\frac{11}{3}N_c - \frac{2}{3}N_f\right)/16\pi^2. \tag{1.3}$$

QCD well consists the experimental data in the perturbative region realized at high temperature (T).

1.2 QCD phase diagram

Since the QCD running coupling decreases with respect to increasing the energy scale, it is natural to consider that the QCD matter at high energy density undergoes the phase transition from a confined state with the chiral symmetry breaking (hadron state) to a deconfined state with the chiral symmetry restoration (quark-gluon plasma state) . Since the typical scale of QCD is $\Lambda_{\rm QCD} \sim 200$ MeV, the quark-hadron transition may take place around temperature $T \sim \Lambda_{\rm QCD}$ or the baryon number density $\rho_{\rm B} \sim \Lambda_{\rm QCD}^3 \sim 1{\rm fm}^{-3}$. In the early universe about 10^{-5} s after the Big Bang, the hot universe has experienced the quark-hadron transition. The core of neutron stars may be the relevant place where dense QCD matter at low temperature would be realized. Experimentally, the heavy-ion collisions in the Relativistic Heavy-ion Collider (RHIC) at Brookhaven National Laboratory (BNL), the Large Hadron Collider (LHC) at CERN and Japan Proton Accelerator Research Complex (J-PARC) at JAEA and KEK provide us with a chance to create hot and/or dense QCD matter.

Figure 1.1 sketches a schematic picture of the QCD phase diagram in the plane of temperature T and quark chemical potential μ_q. At present, our knowledge is limited only in the asymptotically high μ_q region where the perturbative calculation is available, and the small $\mu_q/T << 1$ region where the numerical calculation on lattice is available.

1.3 Chiral symmetry

A nonperturbative feature of QCD is the spontaneous breaking of chiral symmetry. This phenomenon occurs at low energy. As a consequence of the symmetry breaking the gap between hadron and quark mass are explained. For example, current u- and d-quark masses are too light to provide nucleon mass. Now, we consider the fermion part of QCD in the massless limit,

$$\mathcal{L}_q = \bar{q} i\gamma^\mu D_\mu q. \tag{1.4}$$

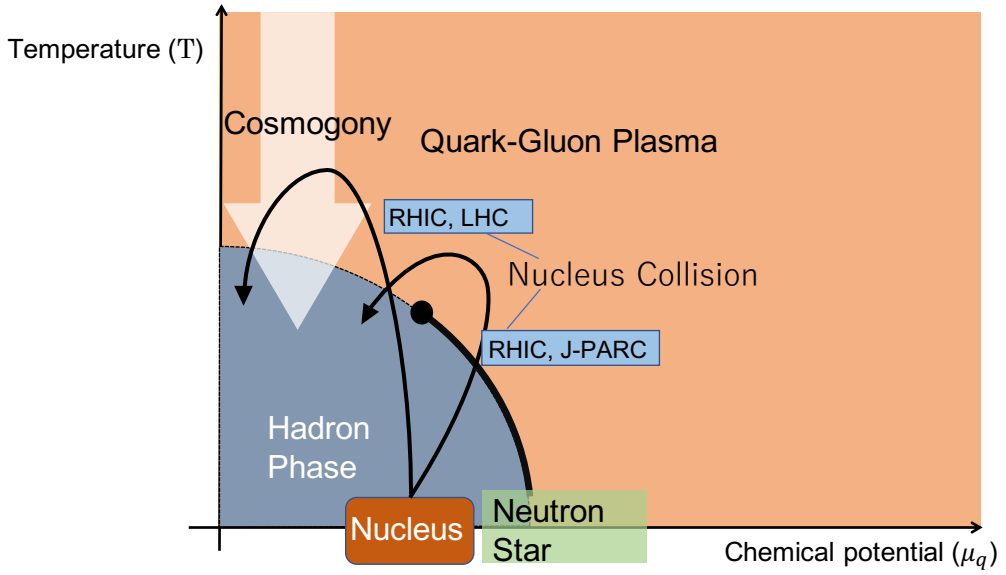

Fig. 1.1: Prediction of QCD phase diagram

Here, the field q can be divided into the left- and right-handed parts based on the chirality operator $\gamma_5 = i\gamma_0\gamma_1\gamma_2\gamma_3$:

$$q_L \equiv \frac{1-\gamma_5}{2}q, \quad q_R \equiv \frac{1+\gamma_5}{2}q. \tag{1.5}$$

The Lagrangian of Eq. (1.4) is then rewritten into

$$\mathcal{L}_q = \bar{q}_L i\gamma^\mu D_\mu q_L + \bar{q}_R i\gamma^\mu D_\mu q_R. \tag{1.6}$$

The Lagrangian (1.6) has invariance under the following phase transformations,

$$q_L \to q'_L = e^{-i\tau^a\theta^a_L}q_L, \quad q_R \to q'_R = e^{-i\tau^a\theta^a_R}q_R. \tag{1.7}$$

where $\theta_{L,R}$ is arbitrary parameters and τ^0 and τ^i (i = 1, 2, 3) are the 2×2 unit and Pauli matrices, respectively. These transformations are elements of the $\mathrm{U_L}(2) \otimes \mathrm{U_R}(2)$ group, and the invariance is called chiral symmetry. The chiral group is decomposed into $\mathrm{U_V}(1) \otimes \mathrm{U_A}(1) \otimes \mathrm{SU_V}(2) \otimes \mathrm{SU_A}(2)$. $\mathrm{U_V}(1)$ symmetry is related to the baryon-number conservation, while $\mathrm{U_A}(1)$ is anomalous in the sense that it is broken by quantum effects. The remainder $\mathrm{SU_A}(2)$ is spontaneously broken when the chiral condensate,

$$\langle\bar{q}q\rangle = \langle\bar{q}_L q_R + \bar{q}_R q_L\rangle, \tag{1.8}$$

is finite. This spontaneous breaking of chiral symmetry generates massless Nambu-Goldstone bosons, and makes quarks massive. The mass is called "dynamical quark mass". Since the current (bare) quark mass is not zero in the real world, chiral symmetry is broken explicitly but weakly.This makes pion massive, although the mass is much lighter than those of other hadrons.

1.4 $\mathbb{Z}_3$ symmetry

One cannot find color charged particles such as quarks and gluons explicitly, but see colorless particles such as pion, proton, and neutron. This phenomenon is called color confinement. This is a representative feature of the non- perturbative QCD vacuum. To describe the confinement-deconfinement transition at finite T, we first introduce an order parameter in the pure Yang-Mills (YM) limit. The YM action for finite T is

$$S_{\rm YM} = \int_0^{1/T} d\tau \int d^3x \frac{1}{4} F^a_{\mu\nu} F^{\mu\nu a}, \tag{1.9}$$

where the gauge field $A^a_\mu(\tau, \mathbf{x})$ has the periodic boundary condition for imaginary direction time τ as

$$A^a_\mu(0, \mathbf{x}) = A^a_\mu(1/T, \mathbf{x}), \tag{1.10}$$

The $S_{\rm YM}$ is invariant under the periodic gauge condition transformation by definition. Also, one can consider the following gauge transformation,

$$A_\mu \to A'_\mu(x) = U(x)(A_\mu(x) + ig\partial_\mu)U^\dagger(x), \tag{1.11}$$

where

$$U(\tau + 1/T, \mathbf{x}) = z_n U(\tau, \mathbf{x}), \tag{1.12}$$

$$U(\tau, \mathbf{x}) \in {\rm SU}(3), \tag{1.13}$$

$$z_n \in \mathbb{Z}_3 \subset {\rm SU}(3). \tag{1.14}$$

The $\mathbb{Z}_3$ is the discrete center subgroup of SU(3) and its element $z_n (n = 0, 1, 2)$ commutes with any element of SU(3). The explicit form of z_n is

$$z_n = e^{2\pi i n/3}, \tag{1.15}$$

with $n = 0$, 1, 2. The transformation (1.11) is called the $\mathbb{Z}_3$ transformation. Because the $\mathbb{Z}_3$ transformation is a part of the gauge transformation, it is one of the symmetry transformations of the YM action (1.9). Therefore the YM partition function is also invariant under the $\mathbb{Z}_3$ transformation, because

it preserves the boundary condition for the gauge field. This is called $\mathbb{Z}_3$ symmetry. Its order parameter is the Polyakov loop,

$$\phi = \frac{1}{3}\mathrm{tr}_c(L), \quad L = \exp\left[i\int_0^{1/T} d\tau A_4\right]. \tag{1.16}$$

The ϕ is transformed under the $\mathbb{Z}_3$ transformation as

$$\phi \to z_n\phi. \tag{1.17}$$

In the heavy quark limit, the expectation value of Polyakov loop $\Phi(\equiv \langle\phi\rangle)$ can be written with the quark free energy F_Q [1];

$$\Phi = e^{-F_Q/T}. \tag{1.18}$$

If $F_Q = \infty$, a single quark can't be produced, and $\Phi = 0$. The system is in the confined phase. In the pure YM theory the conferment-deconfinement transition is thus understood by $\mathbb{Z}_3$ symmetry, and the order parameter is the expectation value of Polyakov loop (Φ). This is summarized as

Confined phase : $\Phi = 0, F_Q = \infty$, $\mathbb{Z}_3$ symmetric state.

Deconfined phase : $\Phi \neq 0, F_Q < \infty$, $\mathbb{Z}_3$ symmetry is spontaneously broken.

1.5 Lattice QCD

Lattice QCD (LQCD) simulation is the first-principle calculation of QCD. In this section, we briefly review the method and its difficulty. LQCD is one of regularization scheme in quantum field theories, in which fermion fields are defined on each lattice site and gauge fields are on each lattice link to preserve local gauge invariance. In LQCD simulations, the path integral is evaluated by the Monte Carlo (MC) method. LQCD simulations successfully reproduce existing experimental values on hadron masses and their decay constants and the qualitative behavior of nuclear force. However, LQCD simulations have the so-called sign problem at finite quark chemical potential (μ_q). For simplicity, we use the notation of continuum QCD without loss of generality. The QCD partition function is given by

$$Z(\mu_q) = \int DADqD\bar{q}\ \exp[-(S_q + S_g)], \tag{1.19}$$

$$S_q \equiv \int d\tau \int d^3\mathbf{x}\ \bar{q}(\gamma_\mu D_\mu + m_0 - \gamma_4\mu_q)q, \tag{1.20}$$

$$S_g \equiv \int d\tau d^3\mathbf{x}\ \frac{1}{4}F^a_{\mu\nu}F^{\mu\nu}_a, \tag{1.21}$$

where the S_q is the fermion action with the covariant derivative D_μ, m_0 is the bare fermion mass and μ_q is the chemical potential. The S_g is the gauge action with the strength $F^a_{\mu\nu}$. The path integration is evaluated by the MC method. Practically, one can use the important sampling method for the gluon-field configuration after integrating the quark field:

$$Z(\mu_q) = \int DA \det M(\mu_q) \exp[-S_g], \tag{1.22}$$

$$M(\mu_q) \equiv \gamma_\mu D_\mu + m - \gamma_4 \mu_q. \tag{1.23}$$

The fermion determinant $\det M(\mu_q)$ should be a real number to use the important sampling method. For finite μ_q, the determinant is not real but satisfies the relation,

$$(\det M(\mu_q))^* = \det M(-\mu_q^*). \tag{1.24}$$

Hence the important sampling method is not feasible at finite μ_q. This is so-called "sign-problem". At $\mu_q = 0$, reality of $\det M(\mu_q = 0)$ is easily derived. Equation (1.24) shows that the fermion determinant is real in the case of pure imaginary chemical potential [2, 3].

1.6 Strategy

A state of matter in high temperature and/or density is defined by the QCD phase diagram. In the QCD phase diagram, a quark-hadron transition line is essential to distinguish hadron state and quark state. In this thesis, we aim to draw a reliable quark-hadron transition line in the QCD phase diagram.

It is also important to elucidate the dynamics of quark-hadron transition for understanding the high-density region of QCD phase diagram where LQCD simulation doesn't work sufficiently. In low density, various thermodynamic quantities were calculated by LQCD simulations. The calculations show that the quark-hadron transition is crossover in low density [4]. However it is difficult to clear the behavior of hadron and quark contributions on various quantities with LQCD simulations. Hence, by using an effective model, we try to clear the dynamics of quark-hadron transition. Then we determine the parameters of the effective model by reproducing LQCD data.

In this thesis, we construct "Hadron-Quark Crossover (HQC) model" by combining Independent Quark (IQ) model and Hadron Resonance Gas (HRG) model. The IQ model (HRG model) describes quark (hadron) state. One can stand for quark and hadron contributions in physical quantities explicitly by using the HQC model. We define the quark-hadron transition by using the HQC model, and draw a QCD phase diagram by the ratio between the number of quarks state and the number of hadron states.

This thesis is constructed as follows: In chapter 2, we construct the HQC model and compare the quark-hadron transition of HQC model with chiral and $\mathbb{Z}_3$ transitions. In chapter 3, we draw a QCD phase diagram with the quark-hadron transition derived by the HQC model. In chapter 4, we summarize the present study.

Chapter 2

Effective model approach for quark-hadron transition

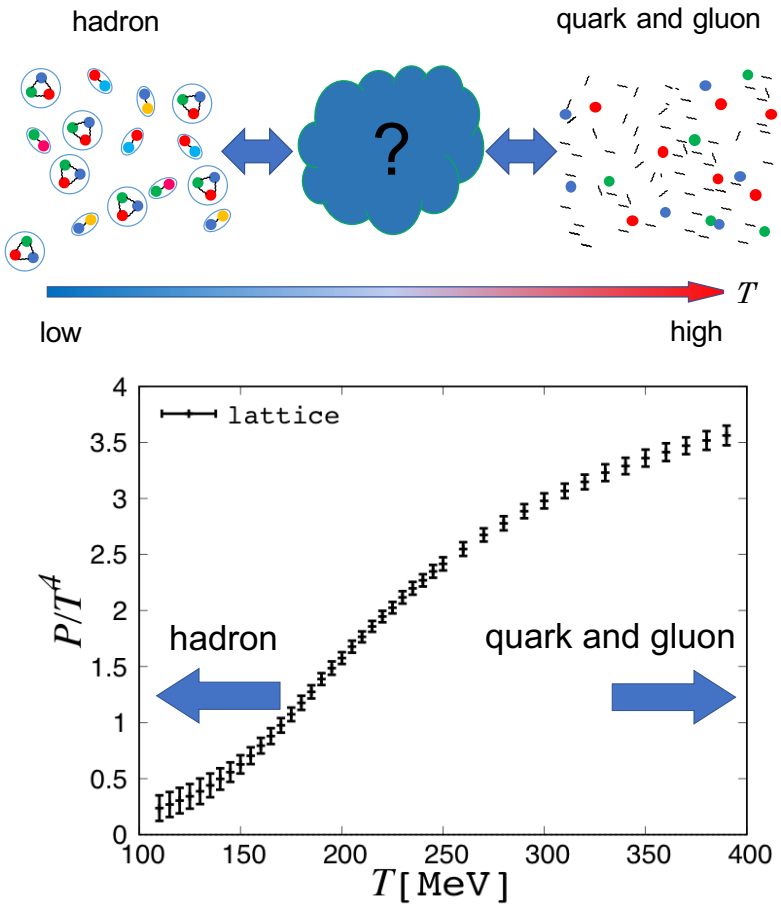

Fig. 2.1: Schema of quark-hadron crossover (upper panel) and pressure of lattice QCD simulation in Ref. [11] (lower panel)

2.1 Introduction

It has been predicted by N. Cabibbo and G. Parisi [5] that a transition from hadrons to quarks occurs in the extremely high temperature and/or high pressure density. For example, in high temperature just after Big Bang up to 10^{-5} s, matters were quark-gluon plasma (QGP). Also, in high density as the core of neutron star, it is considered that hadrons melt into quarks. These behaviours in the finite temperature and density are illustrated in Fig. 1.1, and called "quark-hadron transition". For investigating the revolution of universe and the structure of inner core of neutron star, phenomena in which the quark-hadron transition may be important, it is essential to determine the position of a quark-hadron-transition line in the QCD phase diagram. For temperature less than $T \sim 150$ MeV, quarks and gluons are confined into a hadron. For temperature more than $T \sim 250$ MeV, quarks and gluons become QGP. The resent LQCD result showed that the transition between quark and hadron is smoothly continuous [4]. This means that *the quark-hadron transition is crossover*. However, one is not able to find how high temperature hadrons survive from LQCD simulations. Regarding the study to determine the transition temperature of quark-hadron, usually, T dependence of chiral condensate and/or Polyakov loop are regarded as indicators of the quark-hadron transition. Chiral condensate (Polyakov loop) is an order parameter of chiral ($\mathbb{Z}_3$) symmetry. The chiral condensate correlates an effective quark mass, and also the Polyakov loop is related to the excitation energy of solo quark. However, it is unclear how the restoration and the breaking of these symmetries relate to the quark-hadron transition. We discuss the quark-hadron transition by using thermodynamic quantities which are observables. In this thesis, we construct the model which consists with LQCD data, and determine the quark-hadron transition line by using the constructed model. Treating the number of states of quarks and hadrons visibly, we consider instinctively the quark-hadron transition. We use thermodynamic quantities as good indicators of the quark-hadron transition. And based on the model, we suggest a new definition of quark-hadron transition temperature. In Chap. 2, we construct an effective model, and suggest a new definition of quark-hadron transition temperature. We also determine the transition temperature for some thermodynamic quantities. In Chap. 3, we determine the transition line in QCD phase diagram. Using the constructed model, we expand the results of LQCD simulations from zero chemical potential to finite chemical potential.

2.2 Model

2.2.1 Hadron-quark crossover model

The pressure obtained by LQCD simulations in low temperature can be well described by the hadron gas model, while the pressure in high temperature can be described by perturbative QCD (pQCD). In Ref. [6], the authors proposed a new model to describe the pressure P between high temperature and low temperature by introducing a switching function v:

$$\begin{aligned} P &= v(T,\{\mu_{\rm X}\})P_{\rm H}(T,\{\mu_{\rm X}\}) \\ &\quad + [1-v(T,\{\mu_{\rm X}\})]\,P_{\rm Q}(T,\{\mu_{\rm X}\}), \end{aligned} \tag{2.1}$$

where the $P_{\rm H}$ ($P_{\rm Q}$) means the pressure for pure hadrons (quarks and gluons). The hadron contribution $P_{\rm H}$ is calculated with the HRG model. The quark-gluon contribution $P_{\rm Q}$ is obtained by using pQCD [6]. They have introduced the switching function v to combine $P_{\rm H}$ and $P_{\rm Q}$. In the case of $v=0$, we have quark-gluon plasma. The case of $v=1$ corresponds to pure hadronic matter. In the case of $0<v<1$, we have a mixed state of hadrons and quarks. In Ref. [6], they determined the $v(T,\{\mu_X\})$ so as to reproduce LQCD data on P and the interaction measure. The other thermal quantities are obtainable from P. However, this model has two problems for treating the quark-hadron transition. When T dependence of v is determined to reproduce LQCD results, the hadronic contribution of P is decreased in the high temperature region. The entropy density s ($=\partial P/\partial T$) of hadron then becomes negative at high temperature. Hence the hadron contributions are not understood as the degree of freedom. Also, the v controls the quark-hadron transition and depends on the method of renormalization.

To avoid these problems, in this thesis, we start with the entropy density s.

$$s = f_{\rm H}(T,\{\mu_X\})s_{\rm H}(T,\{\mu_X\}) + [1-f_{\rm H}(T,\{\mu_X\})]\,s_{\rm Q}(T,\{\mu_X\}), \tag{2.2}$$

and calculate the other thermal quantities from s [26]. The $s_{\rm H}$ means the entropy density of pure hadronic matter. The $s_{\rm Q}$ is the entropy density of quark-gluon plasma. The models describing $s_{\rm H}$ and $s_{\rm Q}$ are explained in later sections. The transition function $f_{\rm H}$ describes the occupancy of hadron contribution in the system. The range of $f_{\rm H}$ is set as $0 \le f_{\rm H} \le 1$. In this model, the pure hadronic matter (quark gluon plasma) corresponds to $f_{\rm H}=1$ ($f_{\rm H}=0$). We call the model "hadron-quark crossover (HQC) model". In this chapter, we take 2+1 flavor system which is composed of u, d, s quarks and consider isospin symmetry.

2.2.2 Hadron resonance gas model for Hadron phase

We adopt the hadron resonance gas (HRG) model [8, 9] for hadronic contribution $s_{\rm H}$. The HRG model describes non-interacting stable hadrons and resonances. The thermodynamic potential density is obtained as

$$\Omega_{\rm H} = \Omega_{\rm B} + \Omega_{\rm M}, \tag{2.3}$$

where $\Omega_{\rm B}$ means the baryonic part and $\Omega_{\rm M}$ does the mesonic part. Each part is given by

$$\begin{aligned} \Omega_{\rm B} &= -\sum_{i\in{\rm Baryon}} d_{{\rm B},i} T \int \frac{d^3\mathbf{p}}{(2\pi)^3} \Big\{ \log(1+e^{-(E_{{\rm B},i}-\mu_{{\rm B},i})/T}) \\ &\quad + \log(1+e^{-(E_{{\rm B},i}+\mu_{{\rm B},i})/T}) \Big\}; \\ E_{{\rm B},i} &= \sqrt{\mathbf{p}^2 + {m_{{\rm B},i}}^2}, \end{aligned} \tag{2.4}$$

and

$$\begin{aligned} \Omega_{\rm M} &= \sum_{j\in{\rm Meson}} d_{{\rm M},j} T \int \frac{d^3\mathbf{p}}{(2\pi)^3} \Big\{ \log(1-e^{-(E_{{\rm M},j}-\mu_{{\rm M},j})/T}) \\ &\quad + \log(1-e^{-(E_{{\rm M},j}+\mu_{{\rm M},j})/T}) \Big\}; \\ E_{{\rm M},j} &= \sqrt{\mathbf{p}^2 + {m_{{\rm M},j}}^2}, \end{aligned} \tag{2.5}$$

with baryon masses $m_{{\rm B},i}$ and meson masses $m_{{\rm M},j}$, where the subscripts i and j represent kinds of baryon and meson, respectively. The $d_{\rm B,i}$ and $d_{\rm M,j}$ stand for the degeneracy of baryon and meson. The model parameters are $m_{\rm B}, m_{\rm M}, d_{\rm B}, d_{\rm M}$, and are quoted from the 2015-year edition of the Particle Data Book [10], where their hadron masses are considered up to 2.5 GeV.

The chemical potential $\mu_{{\rm B},i}$ ($\mu_{{\rm M},j}$) for the i-th baryon (j-th meson) is defined by

$$\mu_{\rm H} = B\mu_{\rm B} + I\mu_{\rm I} + Y\mu_{\rm Y}. \tag{2.6}$$

where $\mu_{\rm B}$, $\mu_{\rm I}$, $\mu_{\rm Y}$ are chemical potentials for the corresponding conserved charges, i.e., baryon number B, the z component of isospin I, hyper charge Y. Here the subscript H means kinds of hadron (B, i or M, j). For example, the chemical potential of proton $\mu_{\rm p}$ is

$$\mu_{\rm p} = \mu_{\rm B} + \frac{1}{2}\mu_{\rm I} + \mu_{\rm Y}, \tag{2.7}$$

and the chemical potential of pion μ_{π^+} is

$$\mu_{\pi^+} = \mu_{\rm I}. \tag{2.8}$$

From the thermodynamic potential density, we obtain the pressure $P_{\rm B}, P_{\rm M}$ as

$$P_{\rm B} = -\Omega_{\rm B}, \qquad P_{\rm M} = -\Omega_{\rm M}, \tag{2.9}$$

and the entropy density $s_{\rm B}, s_{\rm M}$ as

$$s_{\rm B} = -\left(\frac{\partial \Omega_{\rm B}}{\partial T}\right)_{V,\{\mu_{\rm X}\}}, \qquad s_{\rm M} = -\left(\frac{\partial \Omega_{\rm M}}{\partial T}\right)_{V,\{\mu_{\rm X}\}}, \tag{2.10}$$

with $\{\mu_{\rm X}\} = (\mu_{\rm B}, \mu_{\rm I}, \mu_{\rm Y})$. The total pressure $P_{\rm H}$ and the entropy density $s_{\rm H}$ are then represented by

$$P_{\rm H} = P_{\rm B} + P_{\rm M}, \tag{2.11}$$

$$s_{\rm H} = s_{\rm B} + s_{\rm M}. \tag{2.12}$$

The HRG model reproduces the LQCD data [11] in low temperature without additional parameter. One of the successful examples is the pressure of Fig. 2.2.

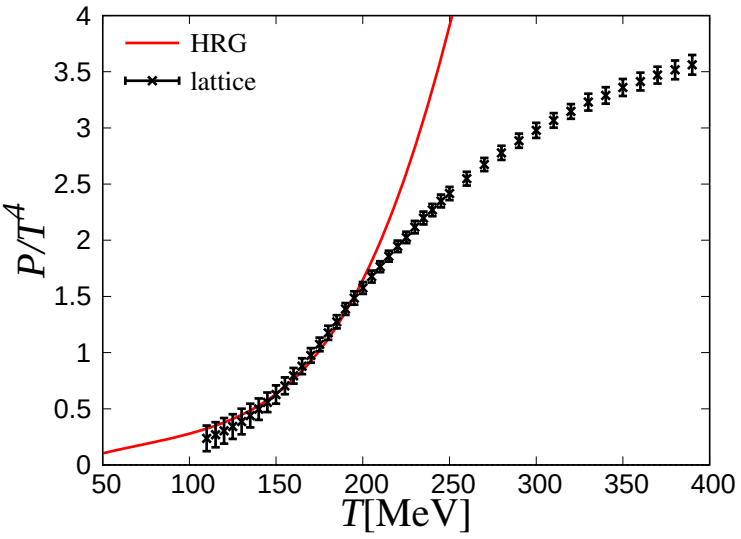

Fig. 2.2: T dependence of the pressure of the HRG model (solid line) and LQCD data (dots with error bars) at $\mu_{\rm B} = \mu_{\rm I} = \mu_{\rm Y} = 0$. The LQCD data are taken from Ref. [11].

2.2.3 Independent Quark model for Quark phase

It is considered that pQCD is the suited method for quark phase in very high temperature. However, we have a problem as follows: In the quark-hadron transition region, pQCD gives uncertainty for the pressure. Then,

to avoid this problem, we propose a new model to be applicable for the region of transition temperature. The model is described as follow. The model describes that quarks propagate in background gluonic fields. The Lagrangian density is given by

$$\mathcal{L}_{\rm Q} = \sum_f \{\bar{q}_f(i\gamma^\mu D_\mu - m_f)q_f\} - \mathcal{U}(T,\Phi,\bar{\Phi}), \tag{2.13}$$

where the subscript f means flavor of quarks as u, d and s. The mass m_f is f-flavored current quark mass. The Covariant derivative is defined by $D_\mu = \partial_\mu - igA^a_\mu \frac{\lambda_a}{2}\delta^{\mu 0}$ with the Gell-Mann matrix λ_a. Namely, we neglect the spatial parts of gluon field and treat its temporal part A_4 as a stationary and uniform background field. The Polyakov loop is then defined by A_4 as follow

$$\Phi = \frac{1}{N_c}{\rm Tr_c} e^{iA_4/T},\ \bar{\Phi} = \frac{1}{N_c}{\rm Tr_c} e^{-iA_4/T}, \tag{2.14}$$

with the number of colors $N_c = 3$ and the trace $\rm Tr_c$ in the color space. The pure gluonic contribution is described by the effective potential $\mathcal{U}$ of the Polyakov-loop. The Polyakov-loop potential $\mathcal{U}$ is given by

$$\frac{\mathcal{U}(T,\Phi,\bar{\Phi})}{T^4} = -\frac{a(T)}{2}\Phi\bar{\Phi} + b(T)\log\{1 - 6\Phi\bar{\Phi} + 4(\Phi^3 + \bar{\Phi}^3) - 3(\Phi\bar{\Phi})^2\}; \tag{2.15}$$

$$a(T) = a_0 + a_1\left(\frac{T_0}{T}\right) + a_2\left(\frac{T_0}{T}\right)^2, \tag{2.16}$$

$$b(T) = b_3\left(\frac{T_0}{T}\right)^3, \tag{2.17}$$

where a_0, a_1, a_2, b_3 and T_0 are the constant parameters. The form of Polyakov potential is derived from the measure of integration of gluon field, see Appendix B . We use the parameter set summarized in Table 2.1. This parameter set has been determined so as to reproduce LQCD data on the equation of state for the pure gluonic system in Ref. [12].

a_0	a_1	a_2	b_3	T_0
3.51	-2.47	15.2	-1.75	270[MeV]

Table 2.1: Parameters of Polyakov-loop potential $\mathcal{U}$ [12].

One can obtain the thermodynamic potential density $\Omega_{\rm Q}$ for the quark phase based on the Lagrangian (2.13), i.e.,

$$\begin{aligned}\Omega_{\rm Q} &= -2\sum_{f=u,d,s}\left[\int_{|\mathbf{p}|\le\Lambda}\frac{d^3\mathbf{p}}{(2\pi)^3}\,3E_f + \int_{|\mathbf{p}|\le\Lambda_{\rm T}}\frac{d^3\mathbf{p}}{(2\pi)^3}(T\log z_f^+ + T\log z_f^-)\right] \\ &+ \mathcal{U}(T,\Phi,\bar{\Phi}),\end{aligned} \tag{2.18}$$

where we introduce the partition functions $z_f^{\pm}$ and the energy E_f as

$$\begin{aligned} z_f^+ &= 1 + 3\bar{\Phi}e^{-(E_f+\mu_f)/T} + 3\Phi e^{-2(E_f+\mu_f)/T} \\ &\quad + e^{-3(E_f+\mu_f)/T}, \qquad (2.19) \\ z_f^- &= 1 + 3\Phi e^{-(E_f-\mu_f)/T} + 3\bar{\Phi}e^{-2(E_f-\mu_f)/T} \\ &\quad + e^{-3(E_f-\mu_f)/T}; \qquad (2.20) \\ & E_f = \sqrt{\mathbf{p}^2 + m_f^2}. \qquad (2.21) \end{aligned}$$

The first term of the right-hand side of Eq. (2.18) stands for the zero-point energy, and the second term is the thermal excitation term. The Λ and $\Lambda_{\rm T}$ mean cutoff for the vacuum and the thermal excitation term, respectively. The Φ and $\bar{\Phi}$ are determined so as to minimize $\Omega_{\rm Q}$. From the thermodynamic potential density $\Omega_{\rm Q}$, we obtain the pressure $P_{\rm Q}$ and the entropy density $s_{\rm Q}$ as follows.

$$\begin{aligned} P_{\rm Q} &= -\Omega_{\rm Q}, \qquad (2.22) \\ s_{\rm Q} &= -\left(\frac{\partial \Omega_{\rm Q}}{\partial T}\right)_{V,\{\hat{\mu}_f\}}, \qquad (2.23) \end{aligned}$$

with $\{\hat{\mu}_f\} = (\mu_{\rm u}, \mu_{\rm d}, \mu_{\rm s})$. In Eq. (2.18), we use the cutoff Λ to regulate the vacuum term

$$\int \frac{d^3\mathbf{p}}{(2\pi)^3}\, 3E_f. \qquad (2.24)$$

It is noted that this vacuum term doesn't affect the thermodynamic quantities since the term is independent of temperature, and is always subtracted in LQCD calculations of P. Hence, we drop the term.

Figure 2.3 shows T dependence of entropy density calculated with the IQ model with cutoff $\Lambda_{\rm T} = 1.95$ GeV and without cutoff ($\Lambda_{\rm T} = \infty$). We find that in no cutoff, the IQ model overestimates the LQCD data in $T >$ 250 MeV. It is reasonable that quark and gluon contributions are small in the low temperature region ($T < 170$ MeV), and rapidly increase around $T = 200$ MeV. We phenomenologically introduced the cutoff $\Lambda_{\rm T}$ into thermal excitation term. The $\Lambda_{\rm T}$ is determined to reproduce the entropy density at $T = 300$ MeV obtained by LQCD simulations. The resultant value is $\Lambda_{\rm T} = 1.95$GeV. Then, $s_{\rm Q}/T^3$ decreases in $T > 300$ MeV, see Fig. 2.4. This means that the IQ model has a limit of application for the temperature range since the $s_{\rm Q}/T^3$ does not reach the Stefan-Boltazmann limit at $T \to \infty$. However, we take no notice of the difficult in this chapter since the IQ model is applicable in $T < 300$ MeV where LQCD data exist. We will discuss the improvement of the IQ model in high temperature range at Chap. 3.

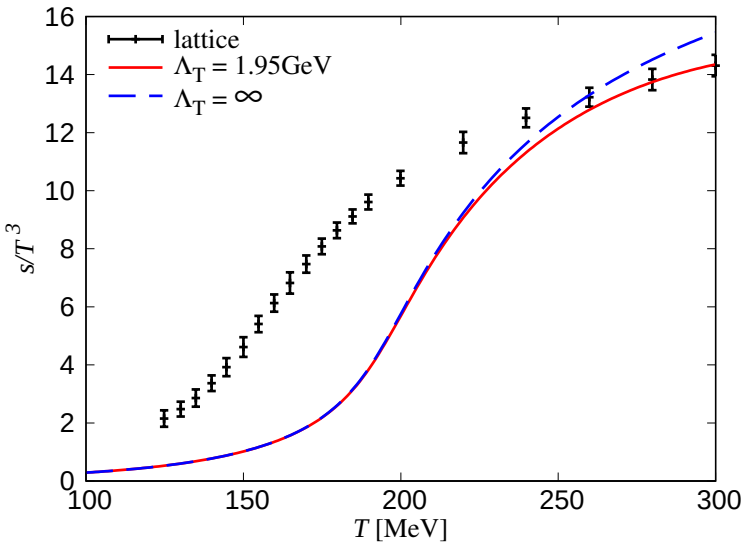

Fig. 2.3: T dependence of the entropy density s of the IQ model with $\Lambda_{\rm T} = 1.95$ GeV (solid line), $\Lambda_{\rm T} = \infty$ (dashed line), and LQCD data (dots with error bars) at $\mu_{\rm B} = \mu_{\rm I} = \mu_{\rm Y} = 0$. The LQCD data are taken from Ref [11].

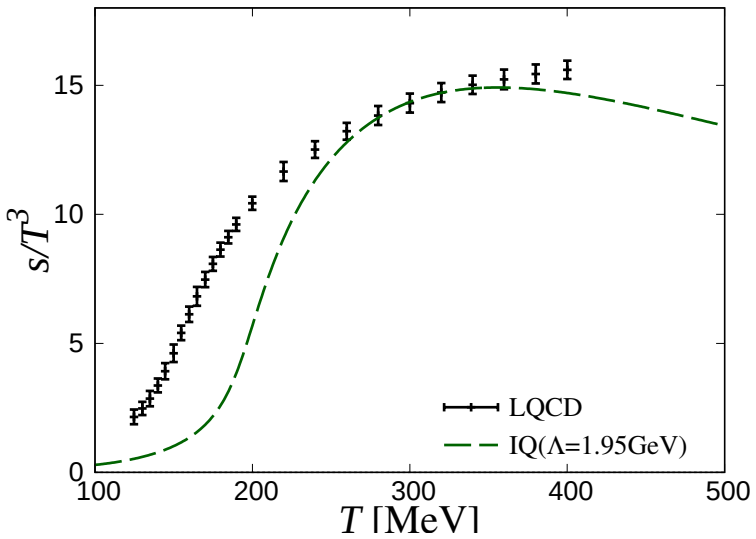

Fig. 2.4: T dependence of the entropy density s in the 2+1 flavor system with zero chemical potential in 100MeV $< T <$ 400MeV. The dashed line means the result of the IQ model for $\Lambda_T = 1.95$ GeV. The LQCD data are taken from Ref [11].

2.3 Numerical results

In this section, we show numerical results in the framework of HQC model. LQCD calculations [11,13–15] showed that the crossover transition occurs on the chiral condensate and the other thermodynamic values. The crossover is a smoothly continuous and mixed transition between hadron state and quark state. It is difficult to define the quark-hadron transition temperature without ambiguity. Here, we determine the quark-hadron transition temperature by comparing the number of quark states with the number of hadron states for any temperature. Comparing the quark-hadron transition temperature with chiral or $\mathbb{Z}_3$ transition temperatures, we show that chiral or $\mathbb{Z}_3$ transitions occur in hadron phase.

2.3.1 Determination of the transition function from entropy density calculated with LQCD simulations

First, we determine the parameters of HQC model. In the HQC model, the calculation of quantities is started from the entropy density with Eq. (2.25),

$$s = f_{\rm H}(T)s_{\rm H}(T) + [1 - f_{\rm H}(T)]\, s_{\rm Q}(T).$$

The value of entropy density corresponds to the number of states in statistical mechanics. The $s_{\rm H}$ is the entropy of pure-hadronic matter and calculated by using the HRG model. The $s_{\rm Q}$ is the entropy of QGP and calculated by using the IQ model. The transition from hadrons to quarks is then shown by $f_{\rm H}$. We assume the explicit form of $f_{\rm H}$ as

$$f_{\rm H}(T) = \frac{1}{2}\left\{1 + \tanh\left((b-T)e^{\left(\frac{c}{T}\right)^d}/a\right)\right\}. \tag{2.25}$$

T dependence of $f_{\rm H}$ is organized by four parameters a, b, c, d, and the value of $f_{\rm H}$ smoothly changes from 1 to 0 as temperature increases; see Fig. 2.2 for schematic figure of $f_{\rm H}$. The parameter b is sensitive to the quark-hadron transition temperature since $f_{\rm H}$ becomes $1/2$ at $T = b$, and QGP and hadrons equally contribute to the entropy. The other parameters a, c and d are used for describing the behavior around $T = b$. The slope of $f_{\rm H}$ is controlled by c, d. The parameter a represents the width of the transition region for our model.

The parameter set of the $f_{\rm H}$ is determined so as to reproduce the entropy density s calculated with the LQCD simulation [11]. Figure 2.6 shows the entropy density s calculated with the HQC model (red line) and the LQCD simulation (dots with error bar). The parameters of $f_{\rm H}$ are determined by

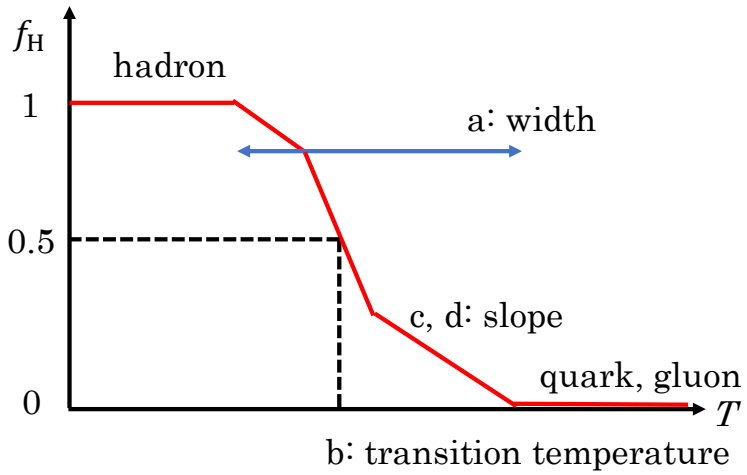

Fig. 2.5: Schema of T dependence of $f_{\rm H}$.

χ^2 fit since the LQCD data have error bars. The obtained parameter set is summarized in Table 2.2. The T dependence of $f_{\rm H}$ is shown in Fig. 2.7. One can see that the quark-hadron transition gets started at $T = 180$ MeV and finished at $T = 260$ MeV.

Here we propose two transition temperature $T_c^{(\rm f_H)}, T_c^{(\rm s)}$. The temperatures $T_c^{(\rm f_H)}$ is defined with $f_{\rm H} = 1/2$. This is the temperature at which the total entropy density s with LQCD simulation is equal to the arithmetical mean of $s_{\rm H}$ and $s_{\rm Q}$,

$$\frac{s_{\rm H} + s_{\rm Q}}{2}, \tag{2.26}$$

and obtained as $T_c^{(f_{\rm H})} = b \simeq 205$ MeV. Another one is defined as follow. The entropy density in Fig. 2.6 is divided into hadron part $f_{\rm H} s_{\rm H}$ (dotted line) and the quark part $(1 - f_{\rm H}) s_{\rm Q}$ (dashed line). The $T_c^{(s)}$ is defined as a temperature at the crosspoint of the quark and hadron parts, i.e., $f_{\rm H} s_{\rm H} = (1 - f_{\rm H}) s_{\rm Q}$. The value thus obtained is $T_c^{(s)} = 215$ MeV. This definition means the balance between the number of hadron states and the number of quark states in the system, since the entropy means the number of states in thermodynamic theory. The difference of about 10 MeV between $T_c^{(\rm f_H)}$ and $T_c^{(\rm s)}$ is not significant since the crossover region $180 < T < 260$ MeV is enoughly broad for containing the difference. Thus, the quark-hadron transition temperature is defined instinctively by the rate of the number of hadron and quark states. Hence, we conclude that $f_{\rm H}$ and s are good indicators of the quark-hadron transition.

a	b	c	d
27.0326[MeV]	205.458[MeV]	174.154[MeV]	17

Table 2.2: Parameters of $f_{\rm H}$.

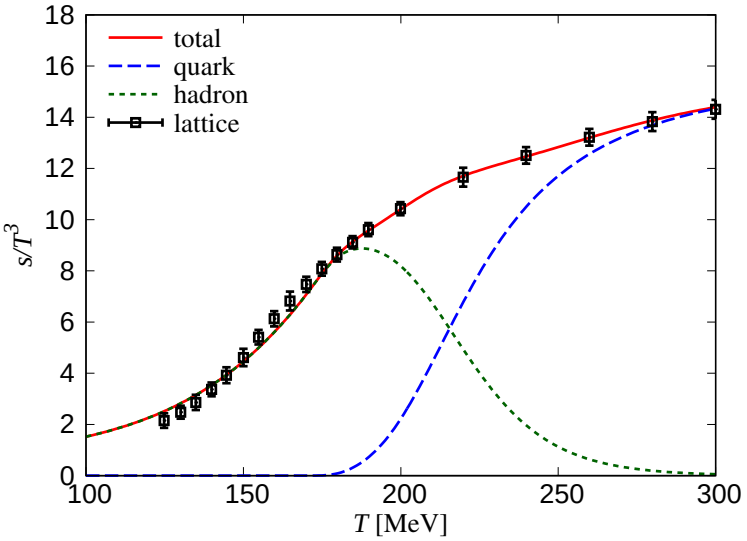

Fig. 2.6: T dependence of the entropy density at $\mu_{\rm B} = \mu_{\rm I} = \mu_{\rm Y} = 0$. The solid line means total value of entropy density in the HQC model framework. The dashed line and dotted line mean quark-gluon contribution and hadron contribution for the HQC-model result. The dots with error bars mean the LQCD data in Ref [11].

2.3.2 Pressure

In Sec. 2.3.1, it is found that $f_{\rm H}$ and s are good indicators of the quark-hadron transition. In this section, we discuss about the relation between the pressure, which is a fundamental quantity, and the quark-hadron transition.

We calculate the pressure P given by the following equation:

$$P(T) - P(T=0) \;=\; \int_0^T dT' s(T'). \tag{2.27}$$

Figure 2.8 shows T dependence of s (left panel) and P (right panel). The figure of s is same as Fig. 2.6, and we set to compare with P. For P, the results of HQC model agree with the LQCD data [11] denoted by dots with error bars.

For determination of transition temperature, the P is divided into the

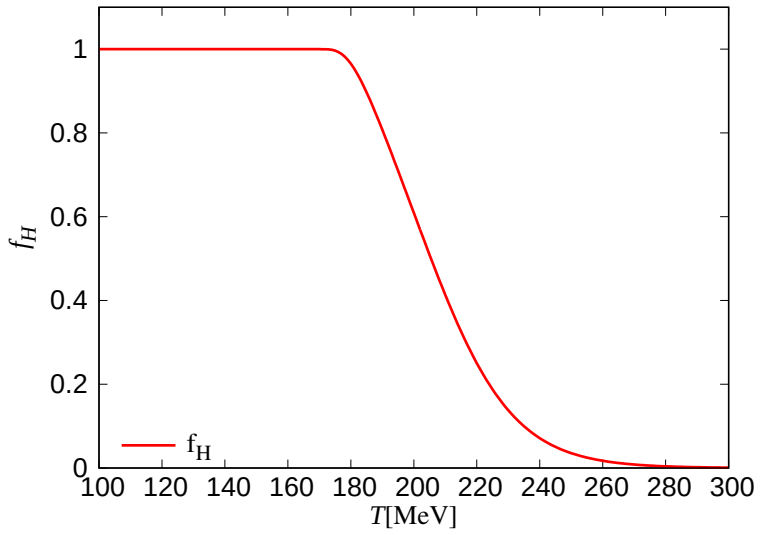

Fig. 2.7: T dependence of the $f_{\rm H}$ at zero chemical potential.

contributions of hadron $P_{\rm Hadron}$ and quark $P_{\rm Quark}$,

$$\begin{aligned} P_{\rm Hadron}(T) &= \int_0^T dT' f_{\rm H}(T') s_{\rm H}(T'), \\ P_{\rm Quark}(T) &= \int_0^T dT' (1 - f_{\rm H}(T')) s_{\rm Q}(T'). \end{aligned} \tag{2.28}$$

The transition temperature is then defined by the condition $P_{\rm Hadron} = P_{\rm Quark}$. The obtained value is $T_c^{(P)} = 249$MeV, and this temperature is obviously higher than $T_c^{(s)} = 215$MeV. Also focusing respective hadron contributions $P_{\rm Hadron}$ and $f_{\rm H} s_{\rm H}$, one can found that $P_{\rm Hadron}$ is not zero for $T > 300$ MeV even though $f_{\rm H} s_{\rm H}$ is almost zero in $T > 280$ MeV.

In our calculation, P is obtained by integrating s from $T = 0$ to T. Hence, even if in high temperature region, P has the contribution of s at the low temperature region. The P shows that the hadron contribution remains even in the high temperature ($T > 280$ MeV). Also, P contains the effect of energy density ϵ beccause of thermodynamic relation, $P = Ts - \epsilon$. The P shows not only the number of states of hadrons or quarks. We conclude that $f_{\rm H}$ and s are better than P to indicate the quark-hadron transition.

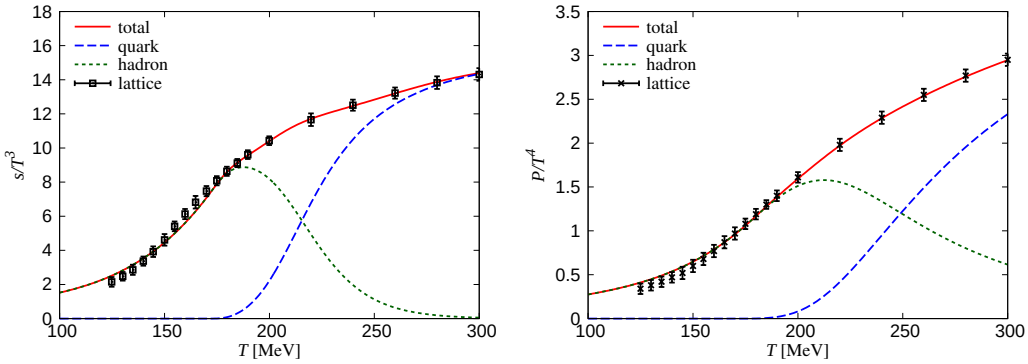

Fig. 2.8: T dependence of the pressure and the entropy density at zero chemical potential. The solid line means the total value for the HQC model. The dotted (dashed) line means hadron (quark) contribution of s and P for the HQC model. The LQCD data (dots with error bars) is taken from Ref. [11].

2.3.3 Interaction measure

Next, we calculate the interaction measure I. The I quantifies the strength of interactions among quarks and gluons and is defined by

$$I = \epsilon - 3P, \tag{2.29}$$

where ϵ means the energy density and is calculated by using the thermodynamic relation,

$$\epsilon = Ts - P, \tag{2.30}$$

for zero chemical potential.

Figure 2.9 shows T dependence of I for LQCD data [11] and the HQC model. The HQC result is represented by a solid line, and LQCD data are denoted by dots with error bars. We see that the HQC-model results consist with the LQCD data. Then it is possible to divide I into the hadron and quark contributions as the cases of s and P. However, such dividing I is not understood physically. Hence, we do not divide I into hadron and quark contributions.

Considering the behavior of I in Fig. 2.9, one can see that interactions among quarks and gluons become weak in high temperature, since the I decreases by the cancellation of ϵ and P in Eq. (2.29). The I also becomes small for $T \to 0$, but the cause is that the total values of s, P are small in low temperature, with Eqs. (2.29) and (2.30). The I then has a maximum around $T = T_{\rm max}^{\rm Int,LQCD} = 200$MeV, which is close to $T_c^{f_{\rm H}} = 205$ MeV. We discuss the coincidence in Sec. 2.3.5.

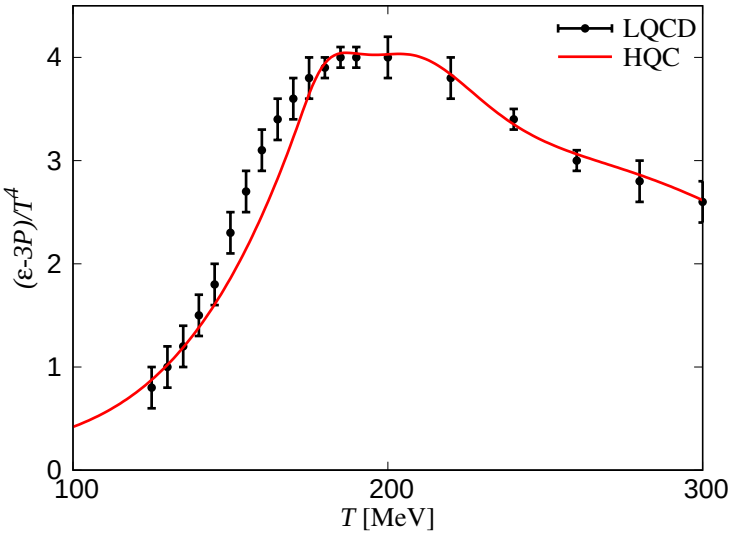

Fig. 2.9: T dependence of the interaction measure at $\mu_{\rm B} = \mu_{\rm I} = \mu_{\rm Y} = 0$. The solid line means the HQC result. The LQCD data (dots with error bars) are taken from Ref [11].

2.3.4 Polyakov loop and renormalized chiral condensate

We showed the consistency of HQC model with LQCD simulations for s, P, I in the previous subsections. Here, we analyze renormalized chiral condensate $\Delta_{\rm l,s}$ and Polyakov loop Φ which are order parameters of chiral and $\mathbb{Z}_3$ transitions.

We first calculate Φ which is the order parameter of $\mathbb{Z}_3$ transition. In pure gauge theory, Φ is related to the excitation energy of solo quark by Eq. (2.14). $\Phi = 0$ ($\Phi = 1$) means that the excitation energy becomes infinity (finite value).

Figure 2.10 shows T dependence of Φ at zero chemical potential. The HQC-model result is represented by a solid line, and dots with error bars stand for LQCD data [15]. Our model result consists with the LQCD data without any adjustable parameter. This means that $\mathbb{Z}_3$ transition can be described quantificaly within the framework of HQC model. With this model, the $\mathbb{Z}_3$ transition temperature $T_c^{\mathbb{Z}_3}$ is determined as the maximum value of $\partial\Phi/\partial T$.

Figure 2.11 shows T dependence of $T_{\rm n} d\Phi/dT$ with $T_{\rm n} = 170$ MeV. The value of $T_{\rm n}$ is the $\mathbb{Z}_3$ transition temperature in LQCD simulations [13,16] for 2+1 flavor system. We found that the $T_{\rm n} d\Phi/dT$ has a peak at $T = 198$ MeV. We then obtain $T_c^{\mathbb{Z}_3} = 198$ MeV, whose value is larger than $\mathbb{Z}_3$ transition temperature of LQCD simulations $T_c^{\mathbb{Z}_3,{\rm LQCD}} = 170 \pm 7$ MeV. However, in

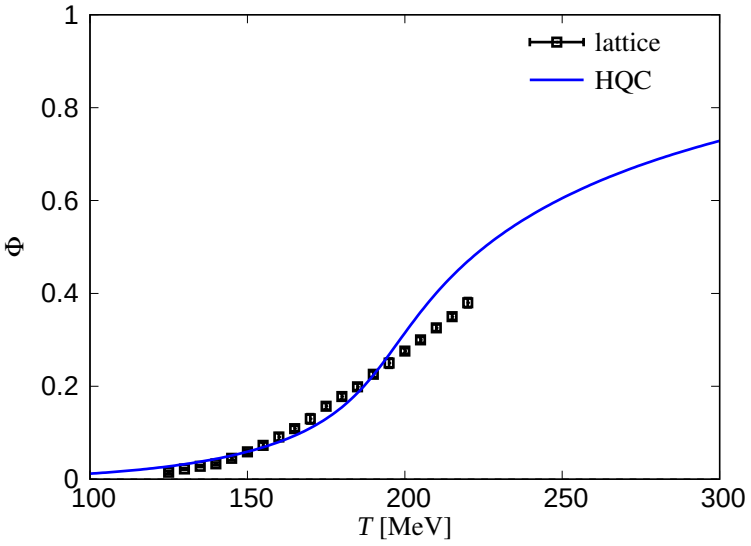

Fig. 2.10: T dependence of the Polyakov loop at $\mu_{\rm B} = \mu_{\rm I} = \mu_{\rm Y} = 0$. The solid line means the HQC-model result. The dots with error bars mean the LQCD data in Ref. [15].

Fig. 2.10, the HQC model roughly reproduces LQCD data on Φ.

Next, we calculate the renormalized chiral condensate $\Delta_{\rm l,s}$:

$$\Delta_{\rm l,s}(T) \equiv \frac{\sigma_{\rm l}(T) - (\frac{m_{\rm l}}{m_{\rm s}})\sigma_{\rm s}(T)}{\sigma_{\rm l}(0) - (\frac{m_{\rm l}}{m_{\rm s}})\sigma_{\rm s}(0)}, \tag{2.31}$$

which is the order parameter of chiral symmetry restoration. $\Delta_{\rm l,s} = 1$ ($\Delta_{\rm l,s} = 0$) means that chiral symmetry of the system is broken (restored). And the σ_l (σ_s) is chiral condensate for light quark (s quark). In the case of $\sigma_l \neq 0$ ($\sigma_s \neq 0$), the chiral symmetry of light quark (s quark) is broken.

We first calculate chiral condensates $\sigma_{\rm l}, \sigma_{\rm s}$ by differentiating pressure P with current quark mass m_f, and derive T dependence of $\Delta_{\rm l,s}$. The chiral condensate σ_f (f=l,s) is obtained as

$$\begin{aligned}
\sigma_f(T) - \sigma_f(0) &= -\frac{\partial}{\partial m_f}\left(P(T, m_f) - P(0, m_f)\right) \\
&= -\frac{\partial}{\partial m_f}\int_0^T dT' \left[(1 - f_{\rm H})s_{\rm Q} + f_{\rm H} s_{\rm H}\right] \\
&= [\sigma_f^{\rm Q}]_0^T + \int_0^T dT' \left[f_{\rm H}\left(\frac{\partial \sigma_f^{\rm H}}{\partial T'} - \frac{\partial \sigma_f^{\rm Q}}{\partial T'}\right)\right],
\end{aligned} \tag{2.32}$$

where we define

$$\sigma_f^{\rm H,Q} = -\frac{\partial P_{\rm H,Q}}{\partial m_f}. \tag{2.33}$$

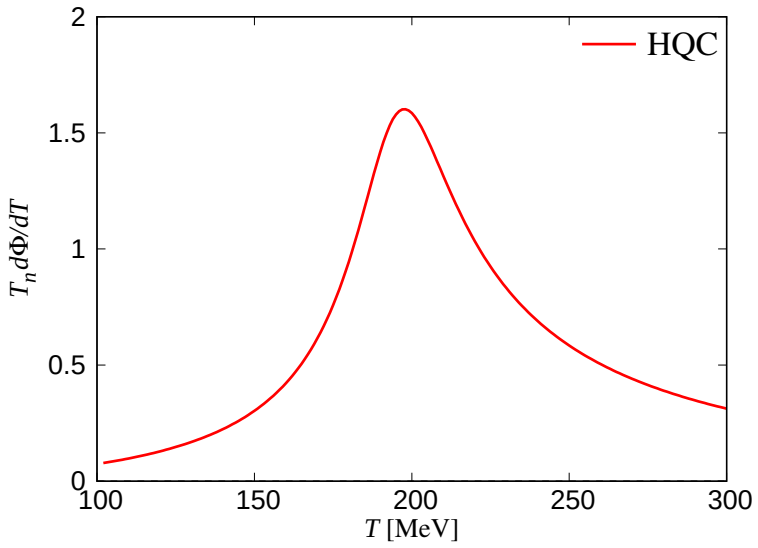

Fig. 2.11: T dependence of the derivative of the Polyakov loop with respect to T at zero chemical potential.

The $\sigma_f^{\rm H}$ ($\sigma_f^{\rm Q}$) means the pure hadronic (quark) contribution of chiral condensate. Here we used

$$\frac{\partial s_{\rm H,Q}}{\partial m_f} = \frac{\partial}{\partial m_f}\frac{\partial P_{\rm H,Q}}{\partial T} = \frac{\partial}{\partial T}\frac{\partial P_{\rm H,Q}}{\partial m_f} = -\frac{\partial \sigma_f^{\rm H,Q}}{\partial T}. \tag{2.34}$$

The hadronic contribution $\sigma_f^{\rm H}$ is written by

$$\begin{aligned}\sigma_f^{\rm H} &= -\frac{\partial P_{\rm H}}{\partial m_f} \\ &= -\sum_{i\in{\rm Baryon}} \frac{\partial M_{{\rm B},i}}{\partial m_f}\frac{\partial P_{\rm H}}{\partial M_{{\rm B},i}} + \sum_{j\in{\rm Meson}} \frac{\partial M_{{\rm M},j}}{\partial m_f}\frac{\partial P_{\rm H}}{\partial M_{{\rm M},j}}.\end{aligned} \tag{2.35}$$

Here we introduce quark-mass m_f dependence to hadron masses $M_{{\rm H},i}$, and $\partial M_{{\rm H},i}/\partial m_f$ is described by using constant parameters $C_f^{{\rm H},i}$:

$$\frac{\partial M_{{\rm H},i}}{\partial m_f} = C_f^{{\rm H},i};\ {\rm H} = {\rm B}, {\rm M}. \tag{2.36}$$

Here, the $C_f^{{\rm H},i}$ corresponds to be the number of quarks inside of hadrons. For example, a proton is composed of 2 up-quarks and 1 down-quark: Then, $C_u^{\rm p} = 2$, $C_d^{\rm p} = 1$ and $C_s^{\rm p} = 0$. For the octet NG bosons, π, K and η mesons, the Gell-Mann-Oakes-Renner (GMOR) relation [17] is used to determine $C_f^{{\rm M},j}$ [15,18].

The renormalized chiral condensate $\Delta_{\rm l,s}$ is defined by

$$\Delta_{\rm l,s}(T,\{\mu_{\rm X}\}) \equiv \frac{\sigma_{\rm l}(T,\{\mu_{\rm X}\}) - (\frac{m_{\rm l}}{m_{\rm s}})\sigma_{\rm s}(T,\{\mu_{\rm X}\})}{\sigma_{\rm l}(0,\{\mu_{\rm X}\}) - (\frac{m_{\rm l}}{m_{\rm s}})\sigma_{\rm s}(0,\{\mu_{\rm X}\})}, \tag{2.37}$$

where $m_{\rm l} = \frac{m_{\rm u}+m_{\rm d}}{2}$ is the average value of current quark mass of light quarks. When one puts $m_{\rm u} = m_{\rm d} = m_{\rm l}$ and uses a quantity

$$\begin{aligned} \Sigma_f(T) &\equiv -\frac{\partial}{\partial m_f}\int_0^T dT' \left[(1-f_{\rm H})s_{\rm Q} + f_{\rm H}s_{\rm H}\right] \\ &= \sigma_f(T) - \sigma_f(0), \end{aligned} \tag{2.38}$$

Eq. (2.37) is rewritten as

$$\Delta_{\rm l,s}(T) = 1 + \frac{\Sigma_{\rm l}(T) - (\frac{m_{\rm l}}{m_{\rm s}})\Sigma_{\rm s}(T)}{\sigma_{\rm l}(0) - (\frac{m_{\rm l}}{m_{\rm s}})\sigma_{\rm s}(0)}, \tag{2.39}$$

where $\sigma_{\rm l}(0), \sigma_{\rm s}(0)$ are derived by the GMOR relation for π and K.

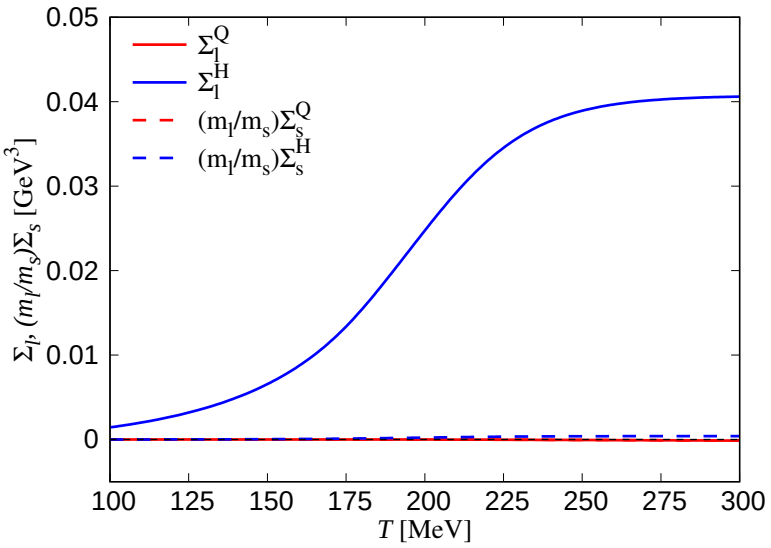

Fig. 2.12: T dependence of $\Sigma_{\rm l}$ and $(m_{\rm l}/m_{\rm s})\Sigma_{\rm s}$ of the numerator of the second term in Eq. (2.39) at zero chemical potential. The solid lines stand for $\Sigma_{\rm l}^{\rm H}$ (blue) and $\Sigma_{\rm l}^{\rm Q}$ (red). The dotted lines stand for $(m_{\rm l}/m_{\rm s})\Sigma_{\rm s}^{\rm H}$ (blue) and $\Sigma_{\rm s}^{\rm Q}$ (red).

Figure. 2.12 shows T dependence of $\Sigma_{\rm l}$ and $(m_{\rm l}/m_{\rm s})\Sigma_{\rm s}$ of Eq. (2.39) in hadron contribution,

$$\Sigma_f^{\rm H}(T) = -\frac{\partial}{\partial m_f}\int_0^T dT' \left[f_{\rm H}s_{\rm H}\right], \tag{2.40}$$

and in QGP contribution,

$$\Sigma_f^{\rm Q}(T) = -\frac{\partial}{\partial m_f}\int_0^T dT' \left[(1-f_{\rm H})s_{\rm Q}\right]. \tag{2.41}$$

Figure 2.12 shows that u, d quarks are included in hadrons mostly contribute for $\Delta_{\rm l,s}$.

Figure. 2.13 shows T dependence of $\Delta_{\rm l,s}$ at zero chemical potential. The HQC-model result explains the LQCD data up to $T = 160$ MeV. Above $T = 170$ MeV, $\Delta_{\rm l,s}$ calculated by our model becomes negative, and this behavior is unphysical since chiral symmetry must be restored in high temperature.

Here, we focus the fact that $\Delta_{\rm l,s}$ of LQCD data almost vanishes at $T_c^{f_{\rm H}} = 205$ MeV. This means that chiral symmetry is already restored in "hadron phase". Hence, it is difficult to explain hadron suppression in $\Delta_{\rm l,s}$ only by using $f_{\rm H}$ (quark-hadron transition), and improvements of HRG model is necessary. We then introduce T dependence of $\partial M_{{\rm B},i}/\partial m_f$ and $\partial M_{{\rm M},j}/\partial m_f$ in Eq. (2.35) as follows:

$$\frac{\partial M_{{\rm B},i}}{\partial m_f} = C_f^{{\rm B},i} g(T), \tag{2.42}$$

$$\frac{\partial M_{{\rm M},j}}{\partial m_f} = C_f^{{\rm M},j} g(T), \tag{2.43}$$

where $g(T)$ is assumed by the following equation,

$$g(T) = \frac{1}{2}\left\{1 + \tanh\left((b_{\rm M} - T)e^{\left(\frac{c_{\rm M}}{T}\right)^{d_{\rm M}}}/a_{\rm M}\right)\right\}. \tag{2.44}$$

The explicit form of $g(T)$ is similar to that of $f_{\rm H}$. The $g(T)$ has four parameters $a_{\rm M}, b_{\rm M}, c_{\rm M}, d_{\rm M}$, which are determined so as to reproduce the LQCD results on $\Delta_{\rm l,s}$. We show resulting parameters in Table 2.3 and T dependence of $g(T)$ in Fig. 2.14. The T dependence of $g(T)$ seems to be reasonable because hadrons should disappear in high T. Figure 2.15 shows the final results of our model on $\Delta_{\rm l,s}$ and Φ. Our model quantitatively agrees with LQCD simulations for both $\Delta_{\rm l,s}$ and Φ.

In the framework of HQC model, we define the chiral transition temperature T_c^χ whose value is determined from a peak position of $\partial\Delta_{\rm l,s}/\partial T$. Obtained value $T_c^\chi = 160$ MeV consists with LQCD data $T_c^{\chi,{\rm LQCD}} = 154 \pm 6$MeV [13, 16].

In this section, we found that the mechanism of quark-hadron transition is different from the mechanism of chiral or $\mathbb{Z}_3$ transitions since $T_c^{(s)} > T_c^\chi, T_c^{\mathbb{Z}_3}$. We obtain this conclusion in first time.

$a_{\rm M}$	$b_{\rm M}$	$c_{\rm M}$	$d_{\rm M}$
66.6654[MeV]	198.644[MeV]	172.781[MeV]	4.78989

Table 2.3: Parameters of g.

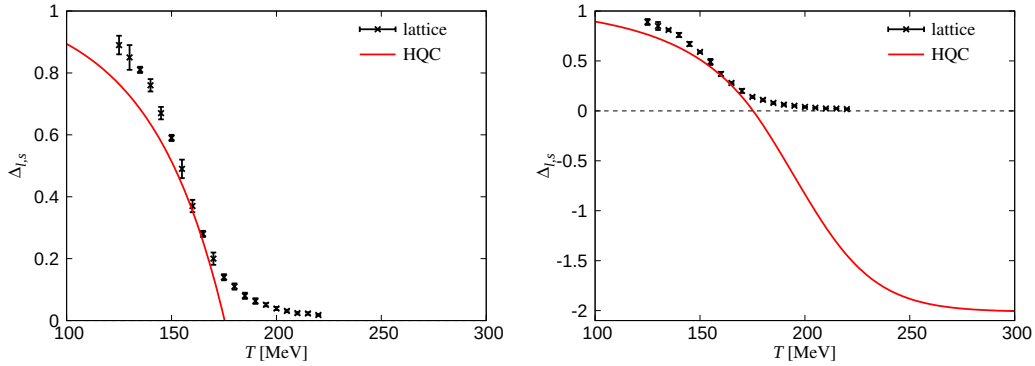

Fig. 2.13: T dependence of the renormalized chiral condensate $\Delta_{\rm l,s}$ at zero chemical potential. The solid line means the HQC-model result. The LQCD data (dots with error bars) is taken from Ref. [15]. The left panel shows the results in $0 < \Delta_{\rm l,s} < 1$, and the right panel shows the results in $-2 < \Delta_{\rm l,s} < 1$.

2.3.5 Transition temperature

In this section, we compare our quark-hadron transition with chiral and $\mathbb{Z}_3$ transition in order to discuss a relationship between the quark-hadron transition and the chiral and $\mathbb{Z}_3$ transitions. About the chiral and $\mathbb{Z}_3$ transition temperatures, we apply the temperatures of LQCD simulations but not those of HQC model since LQCD simulations are reliable than the HQC model. The $\mathbb{Z}_3$ transition temperature of HQC model, $T_c^{\mathbb{Z}_3} = 198$ MeV, is different from the temperature $T_c^{\mathbb{Z}_3,\rm LQCD} = 170 \pm 7$ MeV, but it is not a problem since the HQC model consists with LQCD data on Polyakov loop Φ. We show the transition temperatures $T_c^{(f_{\rm H})}, T_c^{(s)}, T_c^{(P)}$ in the HQC model and $T_c^{\chi,\rm LQCD}$, $T_c^{\mathbb{Z}_3,\rm LQCD}$ in LQCD simulations [13, 16] in Table 2.4.

$T_{\rm c}^{\rm (s)}$	$T_{\rm c}^{\rm (P)}$	$T_c^{(f_{\rm H})}$	$T_c^{\chi,\rm LQCD}$	$T_c^{Z_3,\rm LQCD}$
215[MeV]	249[MeV]	205[MeV]	154± 6[MeV]	170± 7[MeV]

Table 2.4: $T_{\rm c}^{(f_{\rm H})}$, $T_{\rm c}^{(s)}$ and $T_{\rm c}^{(P)}$ are quark-hadron transition temperatures determined from $f_{\rm H}$, s and P. $T_{\rm c}^{\chi,\rm LQCD}$ and $T_{\rm c}^{\mathbb{Z}_3,\rm LQCD}$ are chiral and $\mathbb{Z}_3$ transition temperature of LQCD simulations in Refs. [13, 16].

We find that $T_c^{\chi,\rm LQCD} = 154 \pm 6$ MeV is obviously smaller than $T_{\rm c}^{\rm (s)} = 215$ MeV. In Table 2.4, this result indicates that the chiral symmetry restoration occurs in hadron phase. In fact, in Fig. 2.12, we saw that the rapid decrease of $\Delta_{\rm l,s}$ is mainly induced by light pseudo-scalar mesons in $T < T_c^{\chi,\rm LQCD} = 154 \pm 6$ MeV, and the quark degree of freedom hardly contributes to $\Delta_{\rm l,s}$. It seems that this phenomenon resembles "partial restoration of chiral symmetry" in nuclear matter [19]. In fact, the QCD sum rule at finite density predicts the partial restoration of chiral symmetry even in the normal nuclear matter [20].

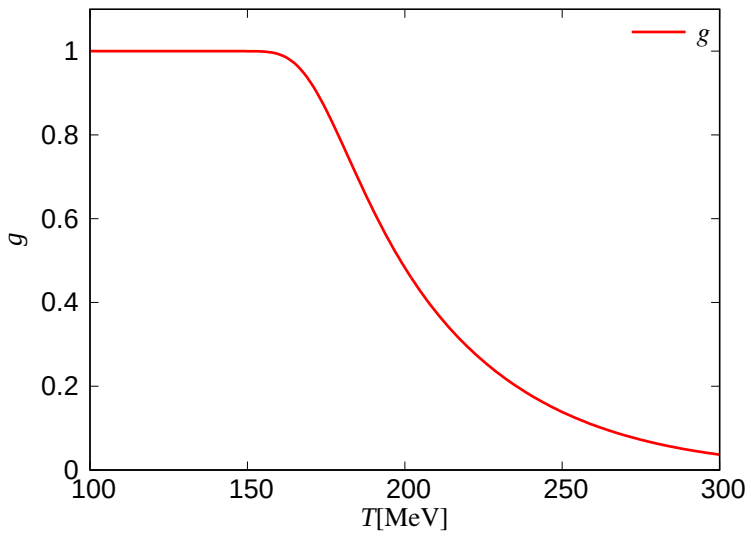

Fig. 2.14: T dependence of $g(T)$.

We conclude that the chiral restoration observed in LQCD simulations does not strongly correlate to the quark-hadron transition. It is also noted that our conclusion is quite different from those obtained by NJL-like models [21, 22]. In the NJL-like models, the renormalized chiral condensate $\Delta_{\mathrm{l,s}}$ is explained by taking the quark degree of freedom only, and the hadron degree of freedom is neglected. In our model, both quarks and hadrons are explicitly taken into account to analyze LQCD data.

Next, we consider the relation between $T_{\mathrm{c}}^{(\mathrm{s})}$ and $T_{\mathrm{c}}^{\mathbb{Z}_3}$. It is unclear why $T_{\mathrm{c}}^{(\mathrm{s})}$ is obviously larger than $T_c^{\mathbb{Z}_3}$. However, this may indicate simply that $\mathbb{Z}_3$ symmetry is not relevant symmetry for the quark-hadron transition in QCD and the Polyakov loop is not a good indicator for the transition.

Furthermore, it is interesting that $T_c^{(f_{\mathrm{H}})}$ is close to the temperature where the interaction measure is maximum, and interactions among quarks and gluons are strongest there. Hence, this result shows that the quark-hadron transition rapidly proceeds when the quarks and gluons much strongly correlate with each other. The relation between the f_{H} and the interaction measure may be an impressive problem as a future work.

2.4 Short summary

In this chapter, we constructed the quark-hadron crossover model that is combined by the hadron resonance gas model and the independent quark

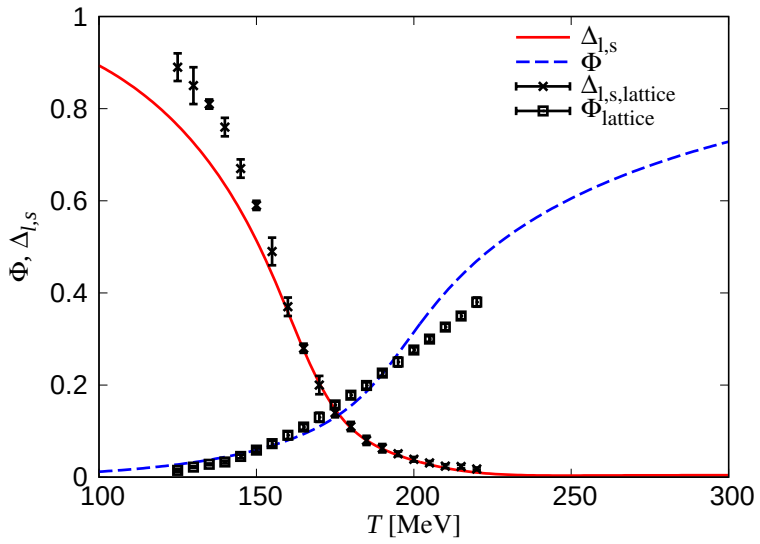

Fig. 2.15: T dependence of the renormalized chiral condensate $\Delta_{\rm l,s}$ and Polyakov loop Φ at $\mu_{\rm B} = \mu_{\rm I} = \mu_{\rm Y} = 0$. The solid line means $\Delta_{\rm l,s}$ of the HQC model. The dashed line means Φ of the HQC model. The HQC-model result is obtained by using the improved model with T dependent $\frac{\partial M_{{\rm B},i}}{\partial m_f}$ and $\frac{\partial M_{{\rm M},j}}{\partial m_f}$. The LQCD data (dots with error bars) are taken from Ref [15].

model. By using the model, we discussed the following four subjects:

1. When do hadrons melt?

2. Determination of quark and hadron contributions for each thermodynamic quantity

3. Relation between the chiral symmetry restoration and the quark-hadron transition

We first determined the quark-hadron transition function $f_{\rm H}$ so as to reproduce LQCD data on T dependence of the entropy density s at zero chemical potential. T dependence of $f_{\rm H}$ indicates that the hadron degree of freedom survives up to $T \sim 250$ MeV.

We divided thermodynamic quantities into the hadron and quark contributions with our model. The quark-hadron transition temperature is defined for three quantities $s, P, f_{\rm H}$. The obtained temperatures are $T_c^{(f_{\rm H})} = 205$ MeV and $T_c^{(s)} = 215$ MeV; $T_c^{(f_{\rm H})}$ is fairly close to $T_c^{(s)}$. This result is reasonable since both $f_{\rm H}$ and s change together with the transition of the degree of freedom in system. On the other hand, $T_c^{(P)} = 249$ MeV is explicitly larger than $T_c^{(f_{\rm H})}$ and $T_c^{(s)}$. The difference can be interpreted that the pressure contains some effects other than the effects of the number of states.

The relation between the chiral symmetry restoration and the quark-hadron transition was discussed. Our model results are consistent with LQCD data on the renormalized chiral condensate $\Delta_{\rm l,s}$ and the Polyakov loop. It is noted that $T_{\rm c}^{\rm (s)}$ is larger than the chiral transition temperature $T_c^\chi = 154 \pm 6$ MeV calculated with LQCD simulation [13, 16]. The gap between $T_{\rm c}^{\rm (s)}$ and T_c^χ indicates "partial restoration of chiral symmetry" in hadron phase.

Chapter 3

QCD phase diagram

In this chapter, by using the Hadron Quark Crossover (HQC) model, we will draw the QCD phase diagram through analyses of the equation of state (EoS) and the susceptibilities.

In the previous chapter, we have constructed the HQC model in order to describe the quark-hadron crossover by the number of hadron and quark states. The HQC model is defined with lattice QCD (LQCD) on the entropy density s as $s = f_{\rm H} s_{\rm H} + (1 - f_{\rm H}) s_{\rm Q}$. The $s_{\rm H}$ ($s_{\rm Q}$) is the entropy density of Hadron Resonance Gas (HRG) model (Independent Quark (IQ) model). The transition function $f_{\rm H}$ is determined from LQCD data on s and susceptibilities for the baryon number (B), the isospin number (I) and the hypercharge number (Y) in the 2+1 flavor system. The HQC model is successful in reproducing LQCD data on the EoS and conserved-charge susceptibilities up to $T = 300$ MeV.

After the calculation in the previous chapter, updated LQCD data [23] is published. The updated data is calculated up to $T = 500$MeV. We calculate the EoS and susceptibilities in the HQC model with the updated LQCD data. However the entropy density s of the present HQC model does not reproduce the updated LQCD results in $T > 300$ MeV, see Fig. 2.4. This disagreement is caused by Λ_T which is the momentum cutoff of the thermal excitation term of thermodynamic potential in the IQ model. The momentum cutoff $\Lambda_{\rm T}$ suppresses quark and gluon contribution for physical quantities in high T. In this chapter, we also improve the IQ model in order to reproduce LQCD data in $T > 300$ MeV.

3.1 Improving Independent quark model

In this subsection, we extend the upper limit of temperature from $T = 300$ MeV to $T = 500$ MeV.

We do not simply extend the IQ model for the high temperature region. In Chap. 2, it was shown that s/T^3 of the present IQ model decreases and disagrees with LQCD data in $T > 300$ MeV, see Fig. 2.4. This means that the original IQ model has a limit of application for the high temperature region where QGP contribution is dominative. Here we improve the IQ model so as to reproduce the entropy density s of LQCD data in $T > 300$ MeV. As a result, this improvement raises reliability of HQC model for QGP description. It is explained that finite $\Lambda_{\rm T}$ causes the decrease of s of the present HQC model in $T > 300$ MeV. In Fig. 3.1, we compare the HQC model for $\Lambda_{\rm T} = 1.95$ GeV with for $\Lambda_{\rm T} = \infty$.

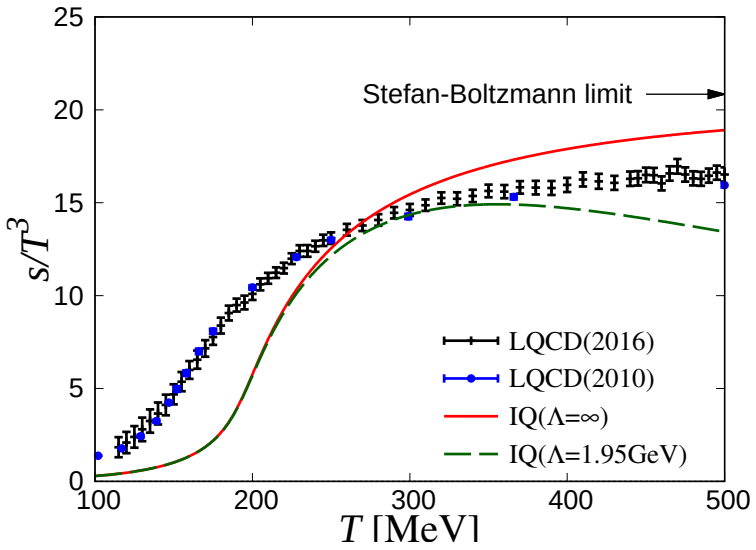

Fig. 3.1: T dependence of the entropy density s in the 2+1 flavor system in 100MeV $< T <$ 500 MeV at zero chemical potential. The solid line means the result of IQ model for $\Lambda_{\rm T} = \infty$. The dashed line means the result of IQ model for $\Lambda_{\rm T} = 1.95$ MeV. The cross dots with error bars are LQCD data in Ref. [23]. The circle dots with error bars are LQCD data in Ref. [11].

Figure 3.1 shows that the s/T^3 of IQ model doesn't decrease for the case of $\Lambda_{\rm T} = \infty$ even in $T > 500$ MeV. However, the result for $\Lambda_{\rm T} = \infty$ overestimates the LQCD data in $T > 300$ MeV. We consider that this is caused by the parameters of Polyakov potential $\mathcal{U}$. The $\mathcal{U}$ controls the value of s in the high T region. The present parameters of $\mathcal{U}$ are determined from s, P, ϵ in pure gauge theory [12]. However, we now consider the system which has dynamical quarks. The dynamical quark effects may be possible to decrease the value of $\mathcal{U}$ in high T. In fact, s of LQCD calculations doesn't reach the Stefan-Boltzmann limit even at $T = 500$ MeV. Hence, we improve the IQ model by changing $a_0 = 3.51$ which is a parameter of $\mathcal{U}$ and controls the high temperature limit value of $\mathcal{U}$. The obtained value is $a_0 = 0.7 \times 3.51 = 2.457$;

see Table 3.1 for the values of new parameters in $\mathcal{U}$. As shown in Fig. 3.2, the result with $a_0 = 2.457$ well explains LQCD data on s in 400MeV $\lesssim T \leq$ 500 MeV.

a_0	a_1	a_2	b_3	T_0
2.457	-2.47	15.2	-1.75	270[MeV]

Table 3.1: Parameters in the improved Polyakov-loop potential $\mathcal{U}$.

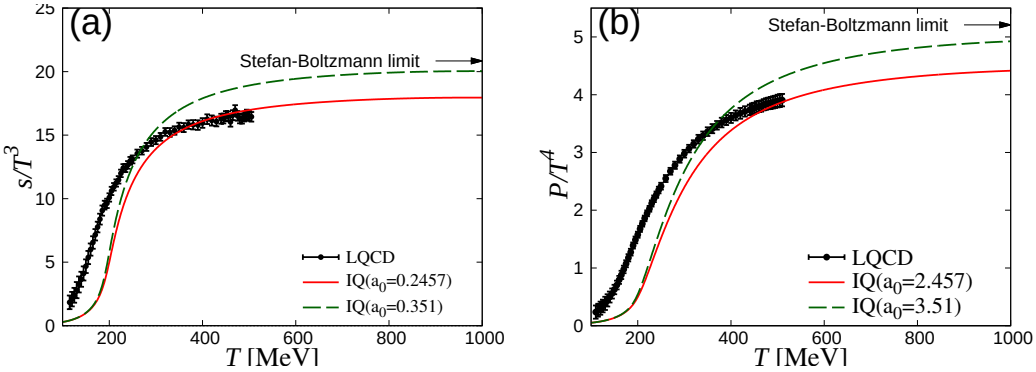

Fig. 3.2: T dependence of the entropy density (a) s and the pressure (b) P for the 2+1 flavor system with zero chemical potential. The dashed line denotes the IQ model with the original value $a_0 = 3.51$, and the solid line corresponds to the IQ model with $a_0 = 2.457$. LQCD data of Ref. [23] are denoted by dots with error bars.

3.2 Improved Hadron quark crossover model

We improved the IQ model in order to explain LQCD data for $T > 300$ MeV. The HQC model is improved by using the new IQ model. In this section, we calculate physical quantities by using the improved HQC model in the 2+1 flavor system. And to draw the QCD phase diagram, we introduce chemical potential dependence to the HQC model. Hereafter, $\{\mu_{\rm X}\}$ means $\{\mu_{\rm B}, \mu_{\rm I}, \mu_{\rm Y}\}$ for the 2+1 flavor system.

For later convenience, we define several kinds of chemical potentials. For the 2+1 flavor system, the chemical potentials of u, d, s quarks are represented by $\mu_{\rm u}, \mu_{\rm d}$ and $\mu_{\rm s}$. These potentials are related to the conserved-charge chemical potentials $\mu_{\rm B}, \mu_{\rm I}, \mu_{\rm Y}$ as

$$\begin{aligned} \mu_{\rm B} &= \mu_{\rm u} + \mu_{\rm d} + \mu_{\rm s}, \\ \mu_{\rm I} &= \mu_{\rm u} - \mu_{\rm d}, \\ \mu_{\rm Y} &= \tfrac{1}{2}(\mu_{\rm u} + \mu_{\rm d} - 2\mu_{\rm s}), \end{aligned} \tag{3.1}$$

for the 2+1 flavor system. For $\mu_{\rm I}$ and $\mu_{\rm Y}$, the coefficients of flavor chemical potentials on the right-hand side of Eq. (3.1) can be the diagonal elements of the matrix representation of Cartan algebra in the special unitary group $SU(3)$, i.e., $\mu_{\rm I} = (1, -1, 0)(\mu_{\rm u}, \mu_{\rm d}, \mu_{\rm s})^{\rm t}$ and $\mu_{\rm Y} = (1/2)(1, 1, -2)(\mu_{\rm u}, \mu_{\rm d}, \mu_{\rm s})^{\rm t}$.

Equation (3.1) gives

$$\begin{aligned} \mu_{\rm u} &= \tfrac{1}{3}\mu_{\rm B} + \tfrac{1}{2}\mu_{\rm I} + \tfrac{1}{3}\mu_{\rm Y}, \\ \mu_{\rm d} &= \tfrac{1}{3}\mu_{\rm B} - \tfrac{1}{2}\mu_{\rm I} + \tfrac{1}{3}\mu_{\rm Y}, \\ \mu_{\rm s} &= \tfrac{1}{3}\mu_{\rm B} - \tfrac{2}{3}\mu_{\rm Y}. \end{aligned} \tag{3.2}$$

The coefficients on the right-hand side of Eq. (3.2) correspond to the quantum numbers of u, d, s quarks. In this sense, the definition (3.1) is natural.

3.2.1 Transition function, entropy density and pressure

First, we introduce chemical potential dependence to the transition function $f_{\rm H}$ in the 2+1 flavor system. Taylor expansion of the transition function $f_{\rm H}(T, \{\mu_{\rm X}\})$ up to the second order with $\{\mu_{\rm X}\}$ is taken as

$$\begin{aligned} f_{\rm H}(T, \{\mu_{\rm X}\}) &= f_{\rm H}^{(0)}(T) + f_{\rm H,B}^{(2)}(T)\left(\frac{\mu_{\rm B}}{T_{\rm n}}\right)^2 + f_{\rm H,I}^{(2)}(T)\left(\frac{\mu_{\rm I}}{T_{\rm n}}\right)^2 + f_{\rm H,Y}^{(2)}(T)\left(\frac{\mu_{\rm Y}}{T_{\rm n}}\right)^2 \\ &\quad + f_{\rm H,BY}^{(2)}(T)\left(\frac{\mu_{\rm B}}{T_{\rm n}}\right)\left(\frac{\mu_{\rm Y}}{T_{\rm n}}\right), \end{aligned} \tag{3.3}$$

where $T_{\rm n} = 170$ MeV is a normalization constant. The value of $T_{\rm n}$ is the $\mathbb{Z}_3$ transition temperature in LQCD simulations [13, 16] for the 2+1 flavor system.

The form of Eq. (3.3) comes from two properties;
(i) $s(= (1 - f_{\rm H})s_{\rm Q} + f_{\rm H}s_{\rm H})$ is invariant under charge conjugation, i.e., the transformation $(\mu_{\rm B}, \mu_{\rm I}, \mu_{\rm Y}) \to (-\mu_{\rm B}, -\mu_{\rm I}, -\mu_{\rm Y})$.
(ii) The system is also invariant under the interchange $\mu_{\rm u} \leftrightarrow \mu_{\rm d}$ (isospin invariant), i.e., the transformation $(\mu_{\rm B}, \mu_{\rm I}, \mu_{\rm Y}) \to (\mu_{\rm B}, -\mu_{\rm I}, \mu_{\rm Y})$.

In particular, for $\mu_{\rm B} = \mu_{\rm I} = \mu_{\rm Y} = 0$, the s reduces to

$$s(T) = f_{\rm H}^{(0)}(T)s_{\rm H}(T) + \{1 - f_{\rm H}^{(0)}(T)\}s_{\rm Q}(T). \tag{3.4}$$

Here, we deduce the equation of $f_{\rm H}^{(0)}$ from Eq. (3.4) and LQCD data on s [23] as follow.

$$f_{\rm H}^{(0)} = \frac{s^{\rm LQCD} - s_{\rm Q}}{s_{\rm H} - s_{\rm Q}}. \tag{3.5}$$

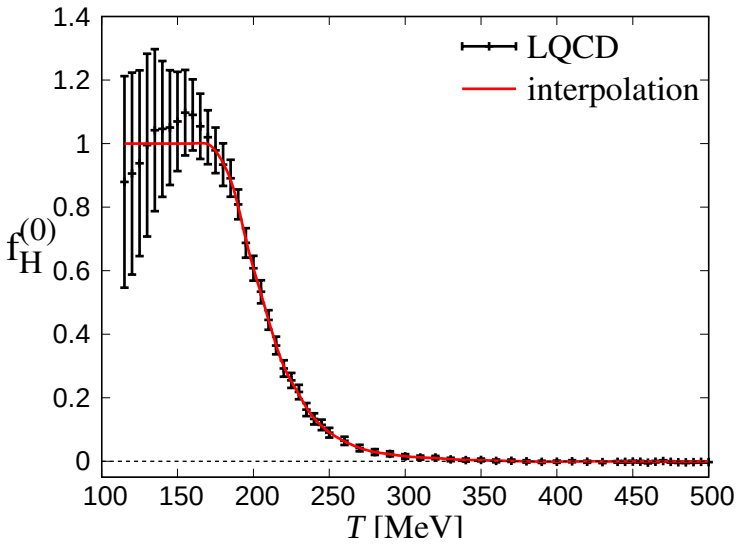

Fig. 3.3: T dependence of $f_{\rm H}^{(0)}(T)$. The solid line is the smooth function obtained with the cubic spline interpolation. LQCD data on $f_{\rm H}^{(0)}$ (dots with error bars) are deduced from those [23] on s by using Eq. (3.4).

In Fig. 3.3, we show the $f_{\rm H}^{(0)}$ (dots with error bars) of Eq. (3.5). The smooth plot which passes through the mean values is made by the cubic spline interpolation for the mean values of LQCD data. Here, the mean values have been taken in 170MeV $\leq T \leq$ 400 MeV where the mean values are set from 0 to 1, and have been set to 0 in $T >$ 400 MeV where the mean values are very small. In $T \leq$ 170 MeV, LQCD data have large error bars and the mean values are not so reliable; in fact, the mean values are accidentally larger than 1 in 140MeV $< T \leq$ 170 MeV. For this reason, we have set the value of $f_{\rm H}$ to 1 in $T \leq$ 170 MeV. The obtained smooth function (solid line) is consistent with LQCD data. Figure 3.3 denotes that the mixed phase appears in 170MeV $\lesssim T \lesssim$ 400 MeV at zero chemical potential.

Figure 3.4 shows T dependence of $s(T)$ and $P(T)$ in $\mu_{\rm B} = \mu_{\rm I} = \mu_{\rm Y} = 0$. Of course, the HQC-model results (solid line) with the $f_{\rm H}^{(0)}(T)$ determined by Eq. (3.3) reproduces LQCD data automatically.

3.2.2 Susceptibilities

In this section, we calculate baryon-, isospin- and hypercharge-number susceptibilities $\chi_{\rm B}, \chi_{\rm I}$ and $\chi_{\rm Y}$ and baryon-hypercharge correlation $\chi_{\rm BY}$ with zero chemical potential. To draw the QCD phase diagram, one should explore the chemical potential dependence of quark-hadron transition as well as temperature dependence. Here, the susceptibilities have the information of the chemical potential dependence even if the data at zero chemical potential. The susceptibility of conserved charges is defined as the second derivative

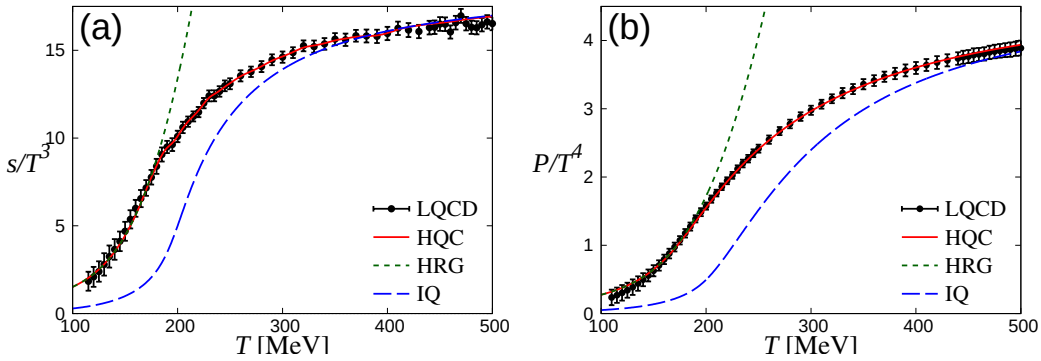

Fig. 3.4: T dependence of the entropy density (a) s and the pressure (b) P calculated by the HQC model for the 2+1 flavor system with zero chemical potential. The solid line is the HQC result with the $f_{\rm H}^{(0)}(T)$ determined in Fig. 3.3. The dotted line stands for the result of the HRG model, the dashed line corresponds to that of the IQ model. In Ref. [23], LQCD data are available for P but not for s. The entropy density s is then evaluated by differentiating P with respect to T.

of P with respect to each charge chemical potential $\mu_{\rm X}$ (X = B, I, Y), i.e., $\chi_{\rm X} = \partial^2 P/\partial\mu_{\rm X}^2$. In the HQC model, the explicit form for susceptibility is

$$\begin{aligned}\chi_{\rm X}(T,\{\mu_{\rm X}\}) - \chi_{\rm X}(0,\{\mu_{\rm X}\}) &= \frac{\partial^2}{\partial\mu_{\rm X}^2}\left[P(T,\{\mu_X\}) - P(0,\{\mu_X\})\right] \\ &= [\chi_{\rm X}^{\rm Q}]_0^T + \int_0^T dT' \left[\frac{\partial^2 f_{\rm H}}{\partial\mu_{\rm X}^2}(s_{\rm H}-s_{\rm Q}) \right. \\ &\quad \left. +2\frac{\partial f_{\rm H}}{\partial\mu_{\rm X}}\frac{\partial(s_{\rm H}-s_{\rm Q})}{\partial\mu_{\rm X}} + f_{\rm H}\frac{\partial^2(s_{\rm H}-s_{\rm Q})}{\partial\mu_{\rm X}^2}\right].\end{aligned} \tag{3.6}$$

In particular at $\{\mu_{\rm X}\} = 0$, we obtain

$$\begin{aligned}\chi_{\rm X}(T) - \chi_{\rm X}(0) &= [\chi_{\rm X}^{\rm Q}]_0^T + \int_0^T dT' \left[\frac{\partial^2 f_{\rm H}}{\partial\mu_{\rm X}^2}(s_{\rm H}-s_{\rm Q}) + f_{\rm H}\frac{\partial^2(s_{\rm H}-s_{\rm Q})}{\partial\mu_{\rm X}^2}\right] \\ &= [\chi_{\rm X}^{\rm Q}]_0^T + \int_0^T dT' \left[2f_{\rm H,X}^{(2)}(s_{\rm H}-s_{\rm Q}) + f_{\rm H}^{(0)}\frac{\partial^2(s_{\rm H}-s_{\rm Q})}{\partial\mu_{\rm X}^2}\right].\end{aligned} \tag{3.7}$$

by using Eq. (3.3).

Similarly, the BY correlation is

$$\begin{aligned}\chi^{(2)}_{\rm BY}(T,\{\mu_{\rm X}\})-\chi^{(2)}_{\rm BY}(0,\{\mu_{\rm X}\}) &= \frac{\partial^2}{\partial\mu_{\rm B}\partial\mu_{\rm Y}}\left[P(T,\{\mu_{\rm X}\})-P(0,\{\mu_{\rm X}\})\right] \\ &= \left[\chi^{\rm Q}_{\rm X}(T,\{\mu_{\rm X}\})\right]^T_0+\int_0^T dT'\Bigg[\frac{\partial^2 f_{\rm H}}{\partial\mu_{\rm B}\partial\mu_{\rm Y}}(s_{\rm H}-s_{\rm Q}) \\ &\quad +\frac{\partial f_{\rm H}}{\partial\mu_{\rm B}}\frac{\partial(s_{\rm H}-s_{\rm Q})}{\partial\mu_{\rm Y}}+\frac{\partial f_{\rm H}}{\partial\mu_{\rm Y}}\frac{\partial(s_{\rm H}-s_{\rm Q})}{\partial\mu_{\rm B}}+f_{\rm H}\frac{\partial^2(s_{\rm H}-s_{\rm Q})}{\partial\mu_{\rm B}\partial\mu_{\rm Y}}\Bigg]\end{aligned} \tag{3.8}$$

for finite $\{\mu_{\rm X}\}$ and

$$\chi^{(2)}_{\rm BY}(T)-\chi^{(2)}_{\rm BY}(0) = \left[\chi^{\rm Q}_{\rm BY}\right]^T_0+\int_0^T dT'\left[f^{(2)}_{\rm H,BY}(s_{\rm H}-s_{\rm Q})+f^{(0)}_{\rm H}\frac{\partial^2(s_{\rm H}-s_{\rm Q})}{\partial\mu_{\rm B}\partial\mu_{\rm Y}}\right], \tag{3.9}$$

for $\{\mu_{\rm X}\}=0$. Other correlation susceptibilities are prohibited by isospin invariance of the system.

We first analyze the LQCD data on $\chi_{\rm B},\chi_{\rm I},\chi_{\rm Y}$ and $\chi_{\rm BY}$ by using the HQC model with no $\mu_{\rm X}$ (X=B, I, Y) dependence of $f_{\rm H}$, i.e., $f^{(2)}_{{\rm H},\alpha}=0$ (α =B, I, Y, BY).

All the results of HQC model explicitly overestimate the LQCD ones above $T=170$ MeV, as shown in Fig. 3.5. We overcome the disagreement by introducing $f^{(2)}_{{\rm H},\alpha}\neq 0$.

Using Eqs. (3.7) and (3.9), one can determine $f^{(2)}_{\rm H,X}$, $f^{(2)}_{\rm H,BY}$ from LQCD data on $s,\chi^{(2)}_{\rm X},\chi^{(2)}_{\rm BY}$ at $\{\mu_{\rm X}\}=0$, respectively: Namely,

$$f^{(2)}_{{\rm H},\alpha} = \frac{1}{w(s_{\rm H}-s_{\rm Q})}\left[\frac{\partial\chi^{(2),{\rm LQCD}}_\alpha}{\partial T}-(1-f^{(0)}_{\rm H})\frac{\partial\chi^{(2),{\rm Q}}_\alpha}{\partial T}-f^{(0)}_{\rm H}\frac{\partial\chi^{(2),{\rm H}}_\alpha}{\partial T}\right], \tag{3.10}$$

for $\alpha={\rm X},{\rm BY}$, where the superscript "LQCD" means LQCD data, $w=2$ for $\alpha={\rm X}$ and $w=1$ for $\alpha={\rm BY}$, and

$$\chi^{(2),{\rm Q}}_{\rm X}=\left.\frac{\partial^2 P_{\rm Q}}{\partial\mu^2_{\rm X}}\right|_{\{\mu_{\rm X}\}=0},\quad \chi^{(2),{\rm Q}}_{\rm BY}=\left.\frac{\partial^2 P_{\rm Q}}{\partial\mu_{\rm B}\partial\mu_{\rm Y}}\right|_{\{\mu_{\rm X}\}=0}. \tag{3.11}$$

The $f^{(2)}_{{\rm H},\alpha}(T)(\alpha={\rm B,I,Y,BY})$ are deduced from LQCD data [23] on $\chi^{(2)}_\alpha(T)$ by the same procedure with Eq. (3.10). And the cubic spline interpolation is made for the mean values of the $f^{(2)}_{{\rm H},\alpha}(T)$. In $T\leq 127$ MeV, we have simply assumed $f^{(2)}_{{\rm H},\alpha}(T)=0$ since we are not able to obtain LQCD data. In Fig. 3.6, the resulting smooth lines are drawn.

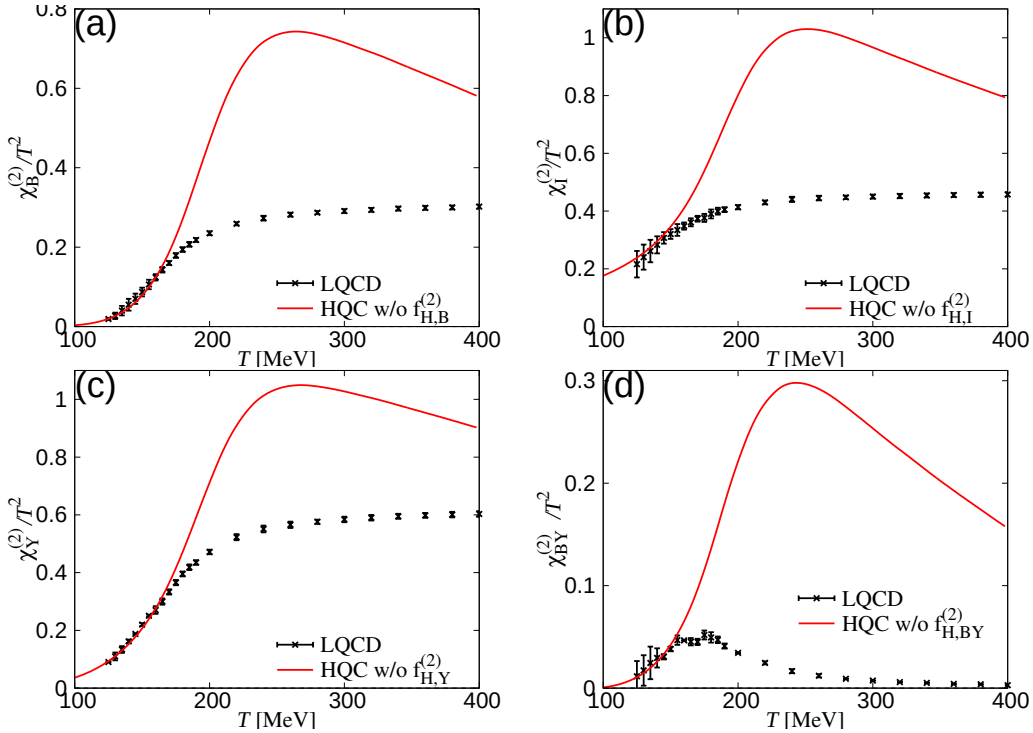

Fig. 3.5: T dependence of the baryon number susceptibility (a) $\chi_{\rm B}$, isospin number susceptibility (b) $\chi_{\rm I}$, hypercharge number susceptibility (c) $\chi_{\rm Y}$ and baryon-hypercharge correlation (d) $\chi_{\rm BY}$ at $\mu_{\rm B} = \mu_{\rm I} = \mu_{\rm Y} = 0$. The solid lines mean HQC-model results without chemical potential dependences of $f_{\rm H}$. The LQCD date (dots with error bars) are taken from Ref. [14].

Figure 3.6 shows that all the $f^{(2)}_{{\rm H},\alpha}(T)$ have same T dependence in $T \gtrsim 200$ MeV. This property plays an important role when we draw the QCD phase diagram in $\mu_{\rm B}$–T, $\mu_{\rm I}$–T, $\mu_{\rm Y}$–T planes. This will be discussed later in Sec. 3.3

In order to confirm the accuracy of the cubic spline interpolation, HQC results (solid line) for susceptibilities are compared with original LQCD data on $\chi^{(2)}_{\alpha}(T)$, see Fig. 3.7. As expected, good agreement is seen between them. The HRG model (dotted line) reproduces the LQCD data in $T \lesssim 170$ MeV, the IQ model (dashed line) is also close to the data at $T = 400$ MeV.

We succeeded in determining $\mu_{\rm X}$ dependence of $f_{\rm H}$. The dependence of flavor chemical potential μ_f (f = u, d, s) are obtained through Eq. (3.1). The $f_{\rm H}$ can be expanded with respect to μ_f (f=u, d, s):

$$f_{\rm H}(T,\{\mu_f\}) \;=\; f^{(0)}_{\rm H}(T) + \sum_{f,f'\in {\rm u,d,s}} f^{(2)}_{{\rm H},ff'}(T)\left(\frac{\mu_f}{T_{\rm n}}\right)\left(\frac{\mu_{f'}}{T_{\rm n}}\right), \qquad (3.12)$$

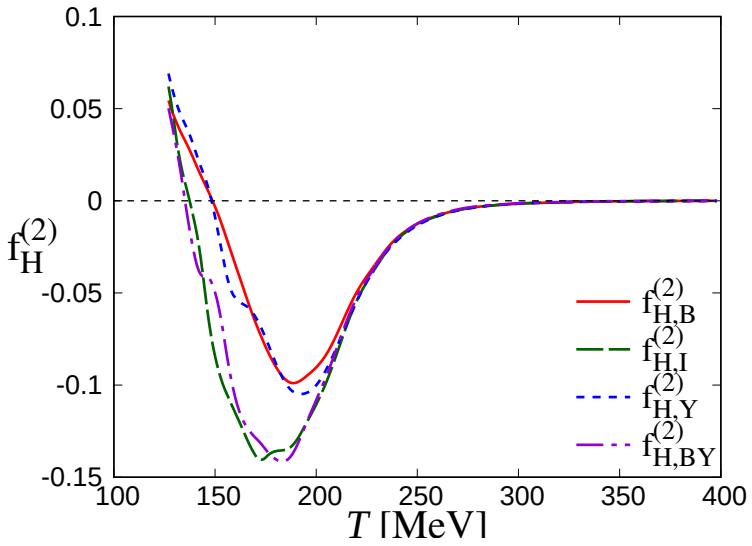

Fig. 3.6: T dependence of $f^{(2)}_{\rm H,X}$ that are deduced from LQCD data [23] on $\chi^{(2)}_{\rm X}$ by using Eq. (3.10). The results are plotted by the solid line for $f^{(2)}_{\rm H,B}$, the dashed line for $f^{(2)}_{\rm H,I}$, the dotted line for $f^{(2)}_{\rm H,Y}$, and the dot-dashed line for $f^{(2)}_{\rm H,BY}$.

with

$$f^{(2)}_{\rm H,uu}(T) = f^{(2)}_{\rm H,B}(T) + f^{(2)}_{\rm H,I}(T) + \frac{1}{4}f^{(2)}_{\rm H,Y}(T) + \frac{1}{2}f^{(2)}_{\rm H,BY}(T), \quad (3.13)$$

$$f^{(2)}_{\rm H,ss}(T) = f^{(2)}_{\rm H,B}(T) + f^{(2)}_{\rm H,Y}(T) - f^{(2)}_{\rm H,BY}(T), \quad (3.14)$$

$$f^{(2)}_{\rm H,ud}(T) = 2f^{(2)}_{\rm H,B}(T) - 2f^{(2)}_{\rm H,I}(T) + \frac{1}{2}f^{(2)}_{\rm H,Y}(T) + f^{(2)}_{\rm H,BY}(T), \quad (3.15)$$

$$f^{(2)}_{\rm H,us}(T) = 2f^{(2)}_{\rm H,B}(T) - f^{(2)}_{\rm H,Y}(T) - \frac{1}{2}f^{(2)}_{\rm H,BY}(T); \quad (3.16)$$

note that $f^{(2)}_{\rm H,uu}(T) = f^{(2)}_{\rm H,dd}(T)$, $f^{(2)}_{\rm H,ud}(T) = f^{(2)}_{\rm H,du}(T)$ and $f^{(2)}_{\rm H,us}(T) = f^{(2)}_{\rm H,ds}(T)$ from isospin symmetry.

Figure 3.8 shows the $f^{(2)}_{{\rm H},ff'}$ as a function of T that are derived from the $f^{(2)}_{{\rm H},\alpha}$ by using Eqs. (3.13)–(3.16). We find that all $|f^{(2)}_{{\rm H},ff'}|$ $(f, f' = u, d, s)$ have a peak around $T = 200$ MeV like $f^{(2)}_{{\rm H},\alpha}$ (α = B, I, Y, BY). On the other hand, the values of $f^{(2)}_{{\rm H},ff'}$ are different from each other unlike $f^{(2)}_{{\rm H},\alpha}$. This fact suggests that the cause of the $f^{(2)}_{{\rm H},\alpha}$ agreement is not the restoration of flavor symmetry.

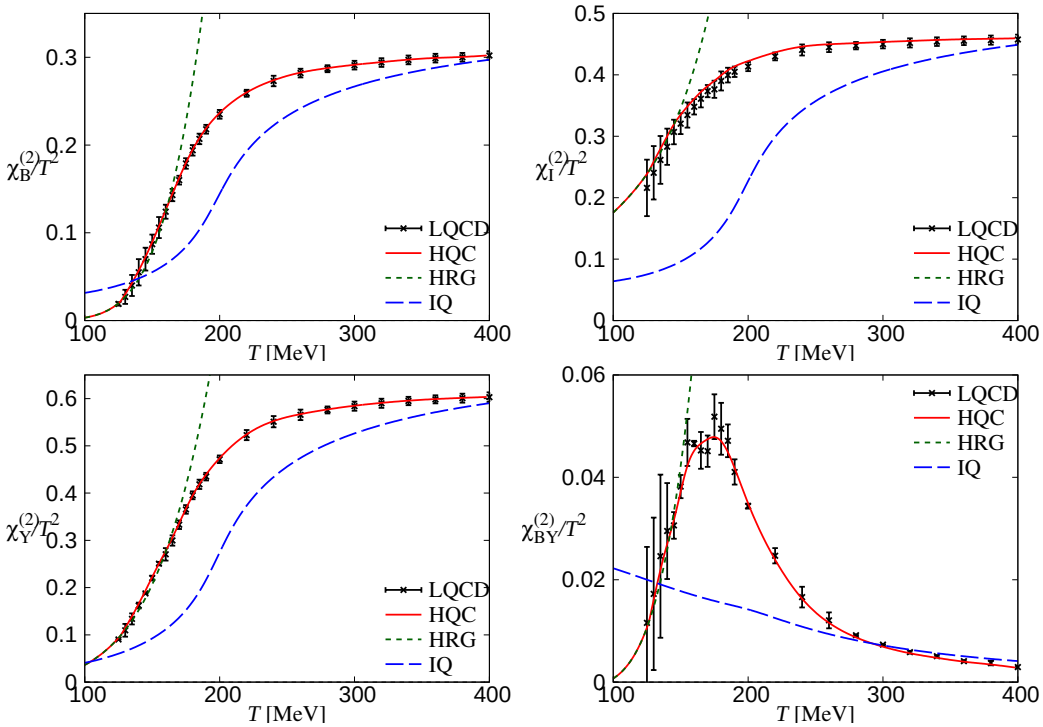

Fig. 3.7: T dependence of the baryon-number B and the isospin I, the hypercharge Y and the BY correlation for the 2+1 flavor system with zero chemical potential. The HQC result is drawn by the solid line. The dotted line stands for the result of HRG model, the dashed line corresponds to that of IQ model. LQCD date (dots with error bars) are taken from Ref. [23].

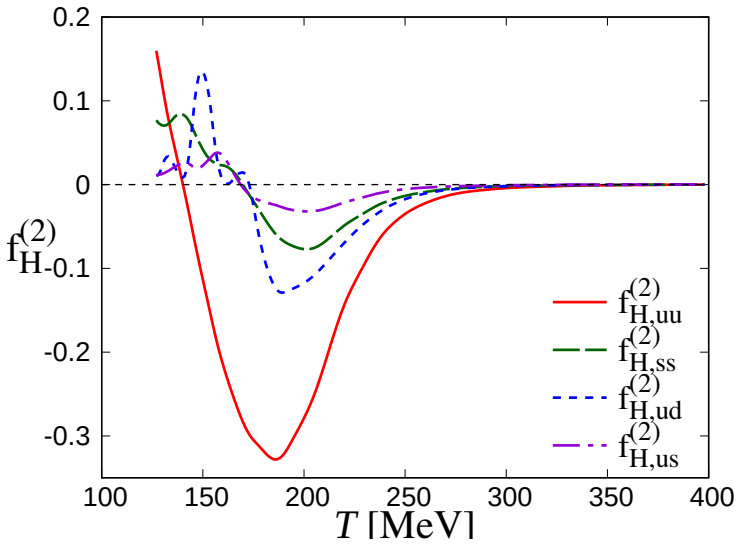

Fig. 3.8: T dependence of $f^{(2)}_{\mathrm{H},ff'}$. The results are plotted by the solid line for $f^{(2)}_{\mathrm{H,uu}}$, the dashed line for $f^{(2)}_{\mathrm{H,ss}}$, the dotted line for $f^{(2)}_{\mathrm{H,ud}}$, and the dot-dashed line for $f^{(2)}_{\mathrm{H,us}}$.

The flavor diagonal and off-diagonal susceptibilities $\chi^{(2)}_{ff'}(T,\{\mu_{\rm X}\})$ are obtained from P of Eq. (2.27) by using Eq. (3.12) as $f_{\rm H}$:

$$\begin{aligned}
&\chi^{(2)}_{ff'}(T,\{\mu_{\rm X}\}) \\
=\ & \frac{\partial^2}{\partial\mu_f\partial\mu_{f'}}P_{\rm Q}(T,\{\mu_{\rm X}\}) \\
&+\int_0^T dT'\left[\frac{\partial^2 f_{\rm H}}{\partial\mu_f\partial\mu_{f'}}(s_{\rm H}-s_{\rm Q})+\frac{\partial f_{\rm H}}{\partial\mu_f}\frac{\partial(s_{\rm H}-s_{\rm Q})}{\partial\mu_{f'}}+\frac{\partial f_{\rm H}}{\partial\mu_{f'}}\frac{\partial(s_{\rm H}-s_{\rm Q})}{\partial\mu_f}+f_{\rm H}\frac{\partial^2(s_{\rm H}-s_{\rm Q})}{\partial\mu_f\partial\mu_{f'}}\right],
\end{aligned} \tag{3.17}$$

for finite chemical potential and

$$\begin{aligned}
&\chi^{(2)}_{ff'}(T) \\
=\ & \chi^{(2),{\rm Q}}_{ff'}(T,\{\mu_{\rm X}\})|_{\{\mu_{\rm X}\}=0}+\int_0^T dT'\left[w f^{(2)}_{{\rm H},ff'}(s_{\rm H}-s_{\rm Q})+f^{(0)}_{\rm H}\frac{\partial^2(s_{\rm H}-s_{\rm Q})}{\partial\mu_f\partial\mu_{f'}}\right],
\end{aligned} \tag{3.18}$$

for zero chemical potential, where $w=2$ for $f=f'$ and 1 for $f\neq f'$. It is known that the off-diagonal flavor susceptibilities $\chi^{(2),{\rm Q}}_{ff'}(T)$ of the PNJL-type model are negligibly small [24]. Hence, for simplicity of calculation, we put $\chi^{(2),{\rm Q}}_{ff'}(T)=0$ for $f\neq f'$.

In Fig. 3.9, we show T dependence of the flavor diagonal and off-diagonal susceptibilities $\chi^{(2)}_{ff'}$ in the 2+1 flavor system at $\mu_f=0$. The solid line indicates the HQC-model result. The results of the IQ and HRG models are also described by dashed and dotted lines respectively for comparison. The HQC model should reproduce LQCD data on the $\chi^{(2)}_{ff'}$ automatically, because of the consistency between flavor and conserved charge chemical potentials. This is satisfied, in spite of $\chi^{(2),{\rm Q}}_{ff'}=0$, as already mentioned in the previous paragraph. The results mean that $\chi^{(2)}_{ff'}$ is contributed only by hadrons, and $|\chi^{(2)}_{ff'}|>0$ stands for surviving the hadrons. This behavior is understood as quarks have strong correlation in hadron, but the correlation becomes weak by melting the hadron. Hence, the off-diagonal susceptibilities are regarded as the indicator of quark deconfinement. One can note from T dependence of the off-diagonal susceptibilities that most of hadrons disappear at $T=$ 400 MeV. These results mean that the quark-hadron transition finishes at $T\approx 400$ MeV.

3.2.3 transition function for finite chemical potential

Up to the previous section, we obtained temperature and chemical potential dependence of $f_{\rm H}$ with LQCD date for zero chemical potential. In this section,

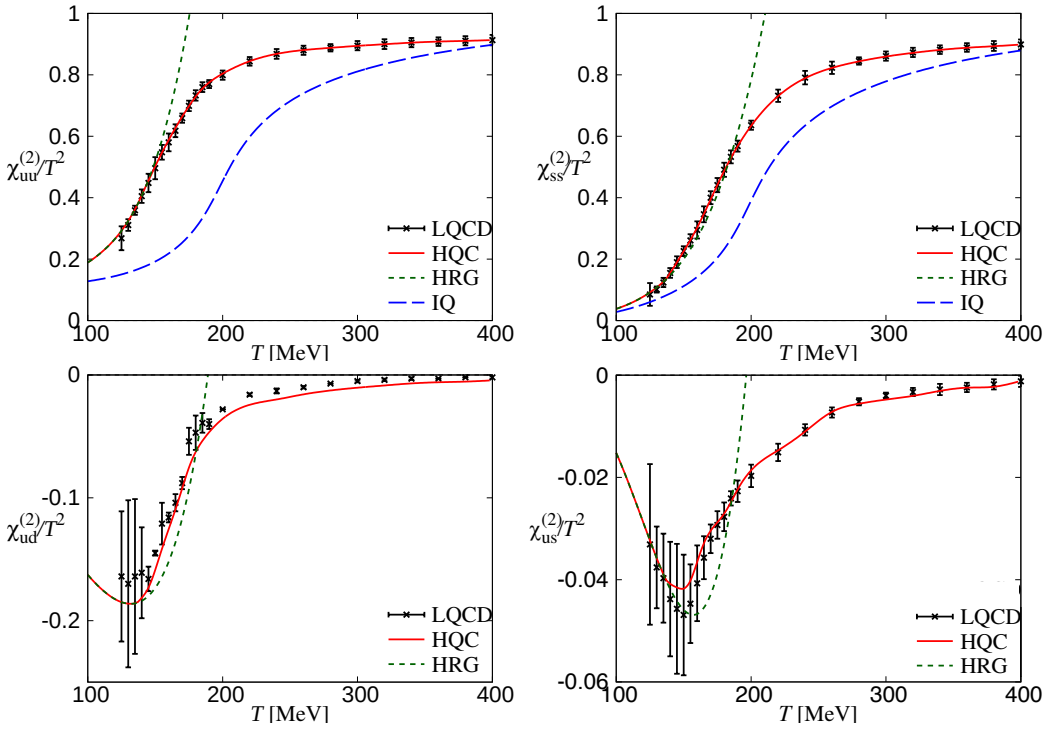

Fig. 3.9: T dependence of diagonal and off-diagonal susceptibilities, $\chi^{(2)}_{ff'}$, in the 2+1 flavor system with zero chemical potential. The HQC result is drawn by the solid line. The dotted line stands for the result of HRG model, the dashed line corresponds to that of IQ model. LQCD data (dots with error bars) are taken from Ref. [14].

we calculate T dependence of $f_{\rm H}$ and the physical quantity in finite chemical potential.

Figure 3.10 shows T dependence of $f_{\rm H}$ for $(\mu_{\rm B}, \mu_{\rm I}, \mu_{\rm Y}) = (0, 0, 0)$ (solid line), $(300[\text{MeV}], 0, 0)$ (dashed line), $(0, 300[\text{MeV}], 0)$ (dotted line), $(0, 0, 300[\text{MeV}])$(dashed dotted line). We find that $f_{\rm H}$ decreases for increasing any $\mu_{\rm X}$ (X=B, I, Y). Hence, hadrons melt more easily, and $f_{\rm H}$ decreases at lower temperature.

Note in particular for $T \gtrsim 200$ MeV, $f_{\rm H}$ has same T dependence for all the results since the T dependence of $f^{(2)}_{\rm H,X}$ have same property. This means that the quark-hadron transition has same reaction for changing any conserved charge numbers in high temperature $T \gtrsim 200$ MeV. We discuss the agreement in high T at Sec. 3.4.

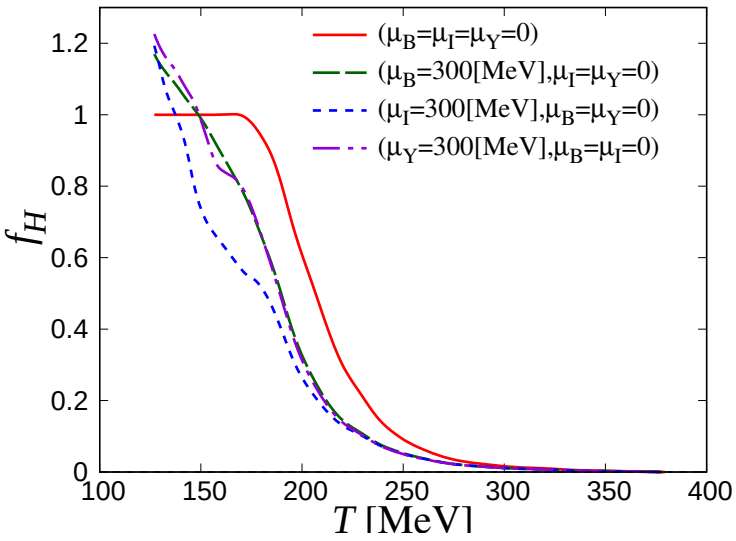

Fig. 3.10: T dependence of the $f_{\rm H}$ at zero chemical potential and finite chemical potential. The solid line shows the result at zero chemical potential. The dashed line means $(\mu_{\rm B}, \mu_{\rm I}, \mu_{\rm Y}) = (300[\mathrm{MeV}], 0, 0)$. The dotted line means $(\mu_{\rm B}, \mu_{\rm I}, \mu_{\rm Y}) = (0, 300[\mathrm{MeV}], 0)$. The dashed line means $(\mu_{\rm B}, \mu_{\rm I}, \mu_{\rm Y}) = (0, 0, 300[\mathrm{MeV}])$.

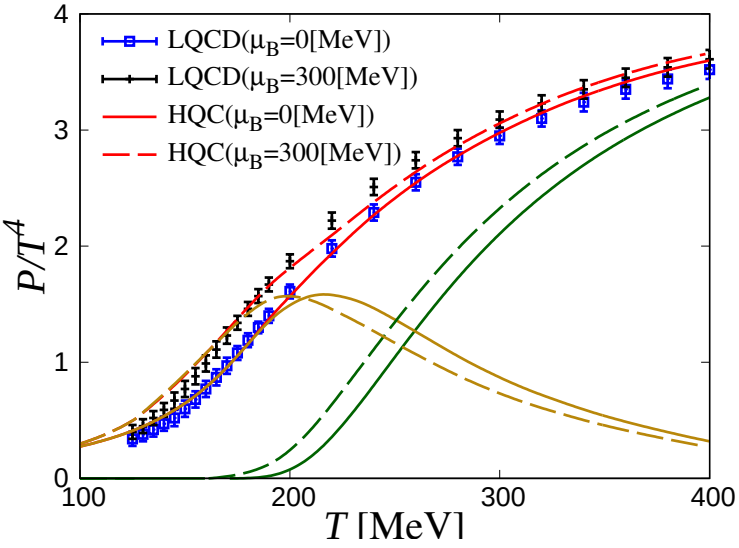

Fig. 3.11: T dependence of the pressure at $(\mu_{\rm B}, \mu_{\rm I}) = (0[\mathrm{MeV}], 0[\mathrm{MeV}])$ and $(\mu_{\rm B}, \mu_{\rm I}) = (300[\mathrm{MeV}], 0[\mathrm{MeV}])$. The solid line shows the HQC-model result at $(\mu_{\rm B}, \mu_{\rm I}) = (300[\mathrm{MeV}], 0[\mathrm{MeV}])$. The dashed line shows the HQC-model result at $(\mu_{\rm B}, \mu_{\rm I}) = (0[\mathrm{MeV}], 0[\mathrm{MeV}])$. The square dots with error bars are LQCD date $(\mu_{\rm B}, \mu_{\rm I}) = (300[\mathrm{MeV}], 0[\mathrm{MeV}])$. The cross dots with error bars are LQCD date $(\mu_{\rm B}, \mu_{\rm I}) = (300[\mathrm{MeV}], 0[\mathrm{MeV}])$. The LQCD data are taken from Ref. [11].

Figure 3.11 shows T dependence of pressure P at $\mu_{\rm B} = 300$ MeV and $\mu_{\rm I} = \mu_{\rm Y} = 0$. The HQC model reproduces the LQCD data very well. In this case, the transition temperature $T_c^{(P)}$ is 245 MeV, and the value is smaller than that of zero chemical potential case $T_c^{(P)} = 259$ MeV.

We conclude that the increase of chemical potential makes the quark-hadron transition temperature decrease.

3.3 QCD phase diagram

We draw the QCD phase diagram in $\mu_{\rm X}-T$ (X=B, I, Y) plane and $\mu_f-T(f = {\rm u, d, s})$ plane.

The transition temperature T_c is defined with $f_{\rm H}(T, \{\mu_{\rm X}\}) = 1/2$. The T_c is also determined for each chemical potential in 0 MeV $< \mu_\gamma <$ 250 MeV, where γ is physical quantities B, I, Y and flavors u,d,s.

Figure 3.12 shows the QCD phase diagram in $\mu_{\rm X}$–T planes. The symbol $T_c(\mu_{\rm X})$ stands for the pseudocritical temperature of the quark-hadron transition in $\mu_{\rm X}$–T plane, where the pseudocritical temperature is defined with $f_{\rm H} = 1/2$.

In virtue of Fig. 3.12, the three transition lines almost agree with each other. Thus, the relation

$$T_c(\mu_{\rm B}) \approx T_c(\mu_{\rm I}) \approx T_c(\mu_{\rm Y}), \tag{3.19}$$

is satisfied in $\mu_{\rm X} <$ 250 MeV. In this thesis, we named the relation (3.19) "BIY approximate equivalence".

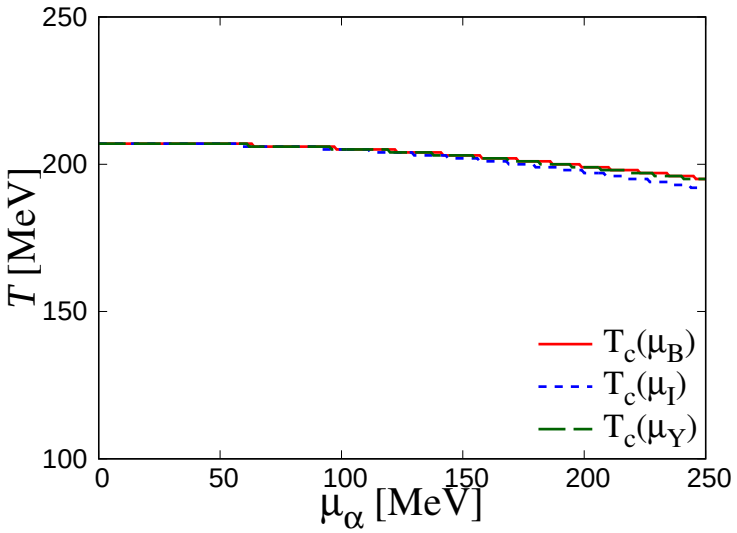

Fig. 3.12: Phase diagram in $\mu_{\rm B}$–T, $\mu_{\rm I}$–T, $\mu_{\rm Y}$–T planes.

BIY approximate equivalence comes from the agreement of $f^{(2)}_{{\rm H},\alpha}$ (α =B, I, Y, BY) in $T \gtrsim 200$ MeV. We discuss this behavior in Sec. 3.4.

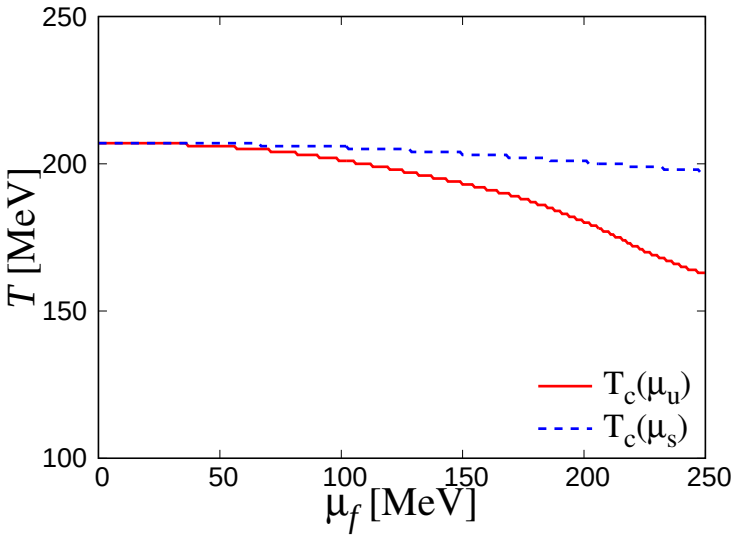

Fig. 3.13: Phase diagram in μ_u–T and μ_s–T planes. Note that $T_c(\mu_{\rm u}) = T_c(\mu_{\rm d})$ $\mu_{\rm u} = \mu_{\rm d}$ because of $f^{(2)}_{\rm H,uu}(T) = f^{(2)}_{\rm H,dd}(T)$ and $f^{(2)}_{\rm H,us}(T) = f^{(2)}_{\rm H,ds}(T)$.

Next, we evaluate the value of the quark-hadron transition temperature for a flavor chemical potential. Figure 3.13 shows the QCD phase diagram in μ_f–T planes. The symbol $T_c(\mu_f)$ stands for the pseudocritical temperature in μ_f–T plane. In the 2+1 flavor system, note that $T_c(\mu_{\rm u}) = T_c(\mu_{\rm d})$ for $\mu_{\rm u} = \mu_{\rm d}$ is established by $f^{(2)}_{\rm H,uu}(T) = f^{(2)}_{\rm H,dd}(T)$ and $f^{(2)}_{\rm H,us}(T) = f^{(2)}_{\rm H,ds}(T)$. Hence, we plotted $T_c(\mu_{\rm u})$ and $T_c(\mu_{\rm s})$ only in Fig. 3.13. The transitions take place at higher T in $\mu_{\rm s}$–T plane than in $\mu_{\rm u}$–T plane. This may stem from the fact that $m_{\rm s} \gg m_{\rm u} = m_{\rm d}$. Hence, u, d quarks are easier to become deconfinement state than s quark for increasing density of the same quark.

We conclude that the quark-hadron transition has flavor dependence in spite of BIY approximate equivalence.

3.4 BIY approximation equivalence

In this section, we discuss BIY approximate equivalence. The BIY approximate equivalence occurs with the agreement of $f^{(2)}_{\rm H,X}$ (X=B, I, Y, BY) in $T \gtrsim 200$ MeV; see Fig. 3.6.

The agreement of $f^{(2)}_{\rm H,X}$ comes from hadron effects, as shown below.

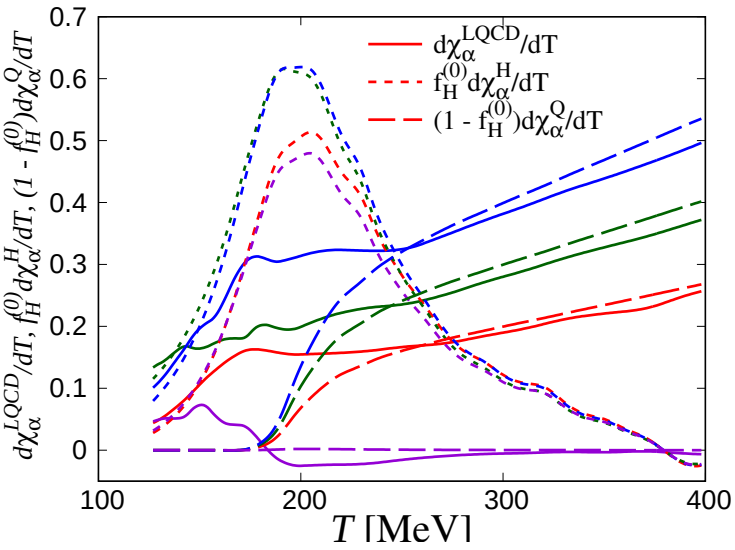

Fig. 3.14: T dependence of contributions for $f^{(2)}_{\mathrm{H},\alpha}$. The solid lines mean results for the HRG model contribution $f^{(0)}_{\mathrm{H}}\partial\chi^{(2),H}_{\alpha}/\partial T$. The dotted lines mean results for the IQ model contribution $(1-f^{(0)}_{\mathrm{H}})\partial\chi^{(2),Q}_{\alpha}/\partial T$. The dashed lines mean results determined from LQCD data $\partial\chi^{(2),\mathrm{LQCD}}_{\alpha}/\partial T$.

Figure 3.14 shows T dependence of $\partial\chi^{(2),\mathrm{LQCD}}_{\alpha}/\partial T$ (solid lines), $(1-f^{(0)}_{\mathrm{H}})\partial\chi^{(2),Q}_{\alpha}/\partial T$ (dashed lines) and $f^{(0)}_{\mathrm{H}}\partial\chi^{(2),\mathrm{H}}_{\alpha}/\partial T$ (dotted lines) in Eq. (3.10). The definition of $f^{(2)}_{\mathrm{H},\alpha}$ is

$$f^{(2)}_{\mathrm{H},\alpha} = \frac{1}{w(s_{\mathrm{H}}-s_{\mathrm{Q}})}\left[\frac{\partial\chi^{(2),\mathrm{LQCD}}_{\alpha}}{\partial T} - (1-f^{(0)}_{\mathrm{H}})\frac{\partial\chi^{(2),\mathrm{Q}}_{\alpha}}{\partial T} - f^{(0)}_{\mathrm{H}}\frac{\partial\chi^{(2),\mathrm{H}}_{\alpha}}{\partial T}\right].$$

We find that the $\partial\chi^{(2),\mathrm{LQCD}}_{\alpha}/\partial T$ and the $(1-f^{(0)}_{\mathrm{H}})\partial\chi^{(2),\mathrm{Q}}_{\alpha}/\partial T$ cancel each other, and the $f^{(0)}_{\mathrm{H}}\partial\chi^{(2),\mathrm{H}}_{\alpha}/\partial T$ agree with each other in high T. Hence, we find that the agreement of $f^{(2)}_{\mathrm{H},\alpha}$ (α = B, I, Y, BY) is caused by hadron contributions.

Also, in the high temperature region $T \gtrsim 200$ MeV, one can define $f^{(2)}_{\mathrm{H},\mathrm{high}T}$ as

$$f^{(2)}_{\mathrm{H},\mathrm{high}T} \equiv f^{(2)}_{\mathrm{H,B}} = f^{(2)}_{\mathrm{H,I}} = f^{(2)}_{\mathrm{H,Y}} = f^{(2)}_{\mathrm{H,BY}}. \tag{3.20}$$

We can then obtain from Eqs. (3.1) and (3.3) that

$$f_{\mathrm{H}} = f^{(0)}_{\mathrm{H}} + f^{(2)}_{\mathrm{H},\mathrm{high}T}(\mu^2_{\mathrm{B}} + \mu^2_{\mathrm{I}} + \mu^2_{\mathrm{Y}} + \mu_{\mathrm{B}}\mu_{\mathrm{Y}}). \tag{3.21}$$

Equation (3.21) shows that μ_{B} and μ_{Y} are exchangeable each other. This means to disappear strangeness number since Y = B + S for hypercharge number Y, baryon number B, strangeness number S. However we are not

able to explain BIY approximate equivalence with only the disappearance of the strangeness number, since $\mu_{\rm I}$ dependence of $f_{\rm H}$ becomes the same dependence as $\mu_{\rm B}$ and $\mu_{\rm Y}$ dependence in high T. Strangeness number don't relate to isospin number.

Hence, it is not easy to explain the agreement of $f^{(2)}_{\rm H,X}$. The BIY approximate equivalence influences experimental phenomenon. This is an interesting future work.

3.5 Short Summary

In this chapter, we discussed the following three subjects:

1. Reconstructing the HQC model of Chap. 2 for updated LQCD data.
2. Introducing the chemical potential dependence to $f_{\rm H}$.
3. Drawing the QCD phase diagram in $\mu_{\rm X} - T$ (X=B, I, Y) planes and $\mu_f - T$ (f=u, d, s) planes.

The Hadron quark crossover (HQC) model is defined by Eq. (2.25). In the model, the hadron contribution $s_{\rm H}(T, \{\mu_{\rm X}\})$ is calculated by the hadron resonance gas (HRG) model, and the quark-gluon contribution $s_{\rm Q}(T, \{\mu_X\})$ is calculated by the independent quark (IQ) model, where $\{\mu_{\rm X}\} = (\mu_{\rm B}, \mu_{\rm I}, \mu_{\rm Y})$.

We improved the IQ model of the previous chapter by using newer LQCD data [14,23] in the 2+1 flavor system. The IQ model in this chapter is rather reliable, since it explains LQCD data on the EoS in 300MeV $\lesssim T$ MeV. This was impossible in chapter 2.

The behavior of $f_{\rm H}(T, \{\mu_{\rm X}\})$ stands for the quark-hadron transition. The $f_{\rm H}(T, \{\mu_{\rm X}\})$ was determined by LQCD data on s for T dependence and the susceptibilities $\chi^{(2)}_{\rm X}$ for $\mu_{\rm X}$ dependence. Accordingly, the improved HQC model automatically reproduces LQCD data on the EoS and the susceptibilities. In particular, the off-diagonal susceptibilities $\chi^{(2)}_{ff'}$ ($f \neq f'$) can be a good indicators to see how hadrons survive as T increases, since the IQ model hardly contributes to the off-diagonal susceptibilities. Hence, $\chi^{(2)}_{ff'} \to 0$ means vanishing hadron contributions. In fact, $\chi^{(2)}_{ff'}$ show that most of hadrons disappear at $T \sim 400$ MeV. We then determined, from T dependence of $f^{(0)}_{\rm H}(T)$ and the off-diagonal susceptibilities, that the transition region is 170MeV $\lesssim T \lesssim 400$ MeV.

In this thesis, we defined the quark-hadron-transition temperature $T_c^{(f_{\rm H})}$ by the condition $f_{\rm H}(T, \{\mu_X\}) = 1/2$. For the 2+1 flavor system with zero chemical potential, $T_c^{(f_{\rm H})}$ is 207 MeV. As mentioned above, the HQC model well explains LQCD data on the EoS and the $\chi^{(2)}_{\rm X}$. In the 2+1 flavor system,

we then drew the phase diagram in $\mu_{\rm B}$–T, $\mu_{\rm I}$–T, $\mu_{\rm Y}$–T planes and found then "BIY approximate equivalence": Namely, the transition lines $T_c(\mu_{\rm X})$ are almost accorded in these planes. We also drew the phase diagram in $\mu_{\rm u}$–T and $\mu_{\rm s}$–T planes. We then found that $T_c(\mu_{\rm u}) < T_c(\mu_{\rm s})$ when $\mu_{\rm u} = \mu_{\rm s}$. This result shows that the quark-hadron transition takes place at higher T for heavier quark. Furthermore, we investigate a cause of BIY approximate equivalence. We found that hadrons mainly contribute to the BIY approximate equivalence, and that the number of strangeness become zero in high T since $\mu_{\rm B}$ and $\mu_{\rm Y}$ are exchangeable in Eq. (3.21). However, it is mysterious that $\mu_{\rm I}$ dependence becomes also the same dependence for $\mu_{\rm B}$ and $\mu_{\rm Y}$ in the $f_{\rm H}$. Hence, it is difficult to explain the cause of BIY approximate equivalence perfectrly.

We conclude that the quark-hadron transition has a flavor dependence, but has BIY approximate equivalence. It is difficult to discover the flavor dependence by experimental approach, hence we suggest LQCD simulations for the flavor dependence.

Chapter 4

Summary and Outlook

Elucidation of QCD phase diagram is important for hadron physics. In particular, the quark-hadron transition line is essential for the QCD phase diagram. In this thesis, we try to treat explicitly the number of quark and hadron states, when determining the quark-hadron transition.

We made the hadron quark crossover (HQC) model which is able to divide thermodynamic quantities into the hadron and quark contributions. Hence, one can treat the numbers of quark and hadron states explicitly by the HQC model. The HQC model is constructed by combining the hadron resonance gas (HRG) model and the independent quark (IQ) model with the transition function $f_{\rm H}$. The HRG (IQ) model well reproduces LQCD data in the low (high) temperature region. The $f_{\rm H}$ means the occupancy of hadron contribution in the system. The $f_{\rm H}$ is determined so as to reproduce the LQCD data on T dependence of entropy density s at zero chemical potentials. T dependence of $f_{\rm H}$ indicates that the hadron degree of freedom survives up to $T \sim 250$ MeV.

We defined the quark-hadron transition temperature in which the hadron contribution is equal to the quark contribution in physical quantities. Actually, the quark-hadron transition temperature is defined for three quantities $s, P, f_{\rm H}$. The temperatures thus obtained are $T_c^{(f_{\rm H})} = 205$ MeV, $T_c^{(s)} = 215$ MeV, and $T_c^{(f_{\rm H})}$ is fairly close to $T_c^{(s)}$. This result is reasonable since both $f_{\rm H}$ and s change together with the transition. In addition, $T_c^{(P)} = 249$ MeV is explicitly larger than $T_c^{(f_{\rm H})}, T_c^{(s)}$. This is understood since the pressure is the product of the degree of freedom and the kinetic contributions. Light hadrons largely contribute to the pressure in high temperature. Hence hadrons contribute even for small $f_{\rm H}$.

We improved the IQ model for new LQCD data [14,23]. The improvement makes the IQ model more reliable. The IQ model explains LQCD data on the EoS in $400 \lesssim T \leq 500$ MeV and is close to the Stefan-Boltzmann limit in the high T limit. We then obtain the transition temperature $T_c^{(f_{\rm H})} = 207$ MeV.

The $f_{\rm H}(T,\{\mu_{\rm X}\})$ was determined by LQCD data on s for T dependence and the susceptibilities $\chi^{(2)}_{\rm X}$ for $\mu_{\rm X}$ dependence. The $f_{\rm H}(T,\{\mu_{\rm X}\})$ is an indicator of quark-hadron transition. The HQC model points out also that the the off-diagonal susceptibilities $\chi^{(2)}_{ff'}$ $(f \neq f')$ is good indicators of quark-hadron transition. The $\chi^{(2)}_{ff'}$ can indicate to see how hadrons survive as T increases, since the IQ model hardly contributes to the $\chi^{(2)}_{ff'}$. Hence, $\chi^{(2)}_{ff'} \to 0$ means vanishing hadrons. And the $\chi^{(2)}_{ff'}$ show that most of hadrons disappear at $T \sim 400$ MeV. We then determined, from T dependence of $f^{(0)}_{\rm H}(T)$ and the off-diagonal susceptibilities, that the transition region is 170MeV $\lesssim T \lesssim$ 400 MeV.

In this thesis, we defined the quark-hadron transition temperature $T_c^{(f_{\rm H})}$ by $f_{\rm H}(T,\{\mu_X\}) = 1/2$. As mentioned above, the HQC model well explains LQCD data on the EoS and the $\chi^{(2)}_{\rm X}$. In the 2+1 flavor system, we drew the phase diagram in $\mu_{\rm B}$–T, $\mu_{\rm I}$–T, $\mu_{\rm Y}$–T planes. Eventually, we found "BIY approximate equivalence". The transition lines $T_c(\mu_{\rm X})$ are almost accorded in these planes. We also drew the phase diagram in $\mu_{\rm u}$–T and $\mu_{\rm s}$–T planes,and found that $T_c(\mu_{\rm u}) < T_c(\mu_{\rm s})$ when $\mu_{\rm u} = \mu_{\rm s}$. This results show that the quark-hadron transition takes place at higher T for heavier quark. Furthermore, we investigate the BIY approximate equivalence. It is found that hadrons mainly contribute to the BIY approximate equivalence. The BIY approximate equivalence suggests that the quark-hadron transition is not affected by s flavor in high T. The cause of BIY approximate equivalence is explained considerably.

We conclude that:

1. The chiral and the $\mathbb{Z}_3$ transition occur in hadron phase.

2. In $\mu_\gamma < 250$ MeV (γ = B, I, Y, u, d, s), the QCD phase diagram has flavor dependence, but not has physical-quantities dependence because of BIY approximate equivalence.

It is difficult to discover the flavor dependence by experiments. Hence we suggest that the approach of LQCD simulations is essential to clarify the flavor dependence.

Acknowledgements

First of all, I would like to express the deepest gratitude to emeritus Prof. Masanobu Yahiro. He guided me how interesting the physics of QCD. He is always supported my research me as a supervisor. I owe my wonderful Master and Doctor Course to his warm encouragement.

I would like to express a deep obligation to Prof. Emiko Hiyama. She took charge me on this thesis. I am very grateful to her.

I would like to thank Prof. Hiroaki Kouno. He gave me several beneficent comments and knowledge with his great insights. His nice indication brings on broading my horizons in physics. I would like to extend my special thanks to Dr. Masahiro Ishii, Dr. Junpei Sugano, Dr. Junichi Takahashi and Master Yuhei Trigoe. Thank to helpful discussions with them, I could obtain much beneficial knowledge and practical techniques such as logical, computational and presentation skills. I appreciate Associate Prof. Yoshifumi Shimizu, Assistant Prof. Takuma Matsumoto and Assistant Prof. Ken-ichi Okumura for useful comments about nuclear physics and elementary particle physics in all the seminars and their lessons.

I show my profound appreciation to Mariko Komori, Yuki Yamaji, Yuko Megumi, Saori Shigematsu, Hiromi Tsuchijima, Megumi Ieda, Noriko Taguchi, Mayumi Takaki, Atsuko Sono, Mariko Komiya, Kanako Mariko, Masako Hirokawa and Asuka Ishibashi for their practical supports.

This work was supported by Grants-in-Aid for Scientific Research (No. 27-3944) from the Japan Society for the Promotion of Science (JSPS).

Finally, I appreciate my grateful family for supporting me through all my life. I owe their supports to accomplish this thesis.

Appendix

A Application to 2+1+1 flavor system

Reference [23] in Ch. 3 has results for 2+1+1 flavor system. 2+1 flavor system has only three kinds of flavor, i.e. u (up), d (down), s (strange). In case of 2+1+1 flavor system, the system includes u,d,s and c (charm). 2+1+1 flavor system is more realistic system than 2+1 flavor system since the real system has six kinds of flavor (u, d, s, c, t (top), b (botom)). However, in thermodynamics, heavier particle is difficult to excite and affects hardly for other light particles. Namely, it is predicted that c quark has too small effects to u, d, s quarks.

In this section, we calculate entropy density s, pressure P, and susceptibilities in 2+1+1 flavor system with $f_{\rm H}$ which determined in 2+1 flavor system. Note that $f_{\rm H}$ is indicator of quark-hadron transition. We estimate the c quark effects for quark-hadron transition by comparing the HQC model calculation with LQCD data in 2+1+1 flavor system.

A .1 HRG model in 2+1+1 flavor system

In 2+1+1 flavor system, the sort of hadrons in the HRG model includes hadron resonances which have charm quark.

Figure A.1 describes entropy density s and pressure P, but for 2+1+1 flavor system with zero chemical potential. The 2+1+1 flavor HRG model well explains LQCD data [23] in the same low T range as the 2+1 flavor model.

A .2 IQ model in 2+1+1 flavor system

In the IQ model, it is very easy to extend from 2+1 flavor system to 2+1+1 flavor system, only adding c quark in the flavor summation term of Eq. (2.13). Since HQC model don't have flavor mixing, the c quark effect is added simply

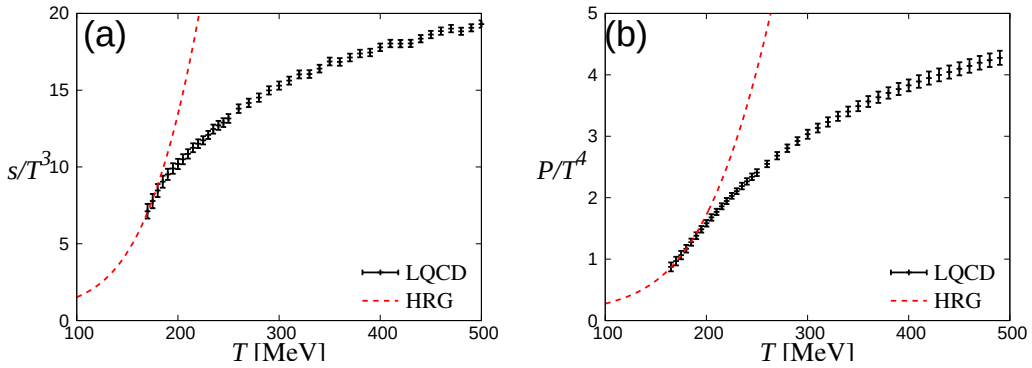

Fig. A.1: T dependence of the entropy density (a) s and the pressure (b) P in the 2+1+1 flavor system with zero chemical potential. The dotted line means the result of the HRG model. In Ref. [23], LQCD data are available for P but not for s. The entropy density s is then evaluated by differentiating P with respect to T.

to the model for 2+1 flavor system. Namely, for the IQ model lagrangian,

$$\mathcal{L}_Q = \sum_{f\in \mathrm{u,d,s}} \bar{q}_f(i\gamma^\mu D_\mu - m_f)q_f - \mathcal{U} \quad \text{for } 2+1 \text{ flavor system}$$
$$\rightarrow \mathcal{L}_Q = \sum_{f\in \mathrm{u,d,s,c}} \bar{q}_f(i\gamma^\mu D_\mu - m_f)q_f - \mathcal{U} \quad \text{for } 2+1+1 \text{ flavor system} \quad \text{(A.1)}$$

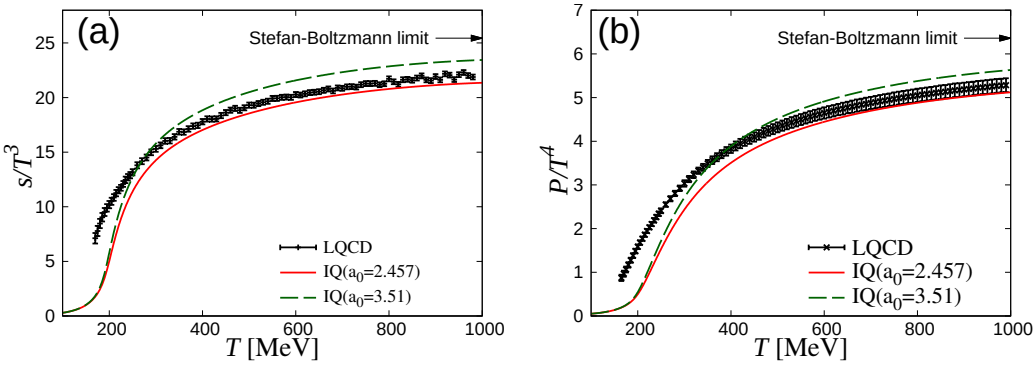

Fig. A.2: T dependence of the entropy density (a) s and the pressure (b) P for the 2+1+1 flavor system with zero chemical potential. The dashed line denotes the IQ model with the original value $a_0 = 3.51$, and the solid line corresponds to the IQ model with $a_0 = 2.457$. LQCD data of Ref. [23] are denoted by dots with error bars.

Figure A.2 shows the same quantity as Fig. 3.2 for the 2+1+1 flavor system. LQCD calculations for P were done in Ref. [23]. We evaluate s from the data by differentiating P with respect to T. Even at $T = 1000$ MeV, LQCD data are about 20% less than the Stefan-Boltzmann limit. The IQ

model with the original value $a_0 = 3.51$ (dashed line) reaches about 90% of the Stefan-Boltzmann limit value at $T = 1000$ MeV. The results of our model with $a_0 = 2.457$ (solid line) reproduce LQCD data in 400MeV $\lesssim T \leq$ 1000 MeV pretty well. Thus, the pure QGP may be realized in $T \gtrsim 400$ MeV also for the 2+1+1 flavor system. The lower limit of the pure QGP can be determined precisely with T dependence of $\chi^{(2)}_{ff'}$ $(f \neq f')$.

A .3 Numerical results for 2+1+1 flavor system

We extend HQC model 2+1 flavor system to 2+1+1 flavor system with the HRG model and the IQ model in 2+1+1 flavor system, but $f_{\rm H}$ is not changed. We then calculate s, P and susceptibilities by using the HQC model.

Entropy density and pressure

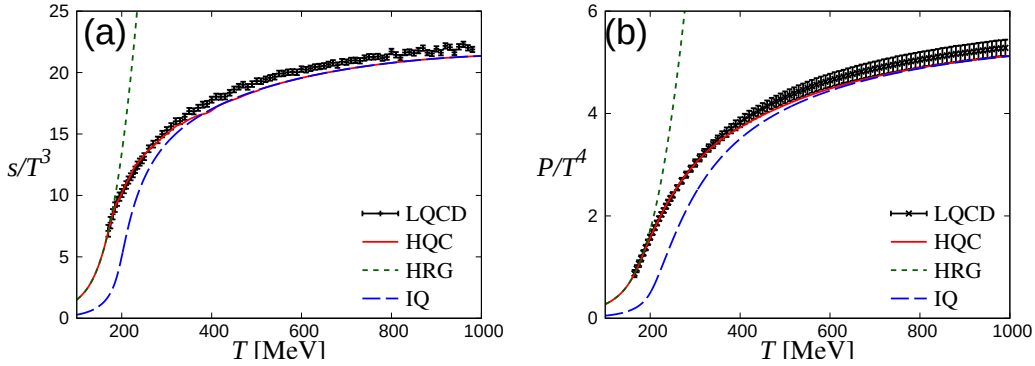

Fig. A.3: T dependence of s and P in the 2+1+1 flavor system with zero chemical potential. The solid line is the result of the HQC model. LQCD data (dots with error bars) are taken from Ref. [23]. The result of the IQ (HRG) model is denoted by a dashed (doted) line.

Figure A.3 shows T dependence of s and P in the 2+1+1 flavor system. The HQC results (solid line) has good agreement with LQCD data (dots with error bars). This agreement supports the assumption $f_{\rm H}^{2+1+1} = f_{\rm H}$.

Flavor susceptibilities

In calculations of susceptibilities for the 2+1+1 flavor system, we define the chemical potential relations by using Cartan algebra in the special unitary

group SU(4) for μ_I, μ_Y and μ_{Y_c}:

$$\begin{aligned}
\mu_B &= \tfrac{3}{4}(\mu_{\rm u} + \mu_{\rm d} + \mu_{\rm s} + \mu_{\rm c}), \\
\mu_I &= \mu_{\rm u} - \mu_{\rm d}, \\
\mu_Y &= \tfrac{1}{2}(\mu_{\rm u} + \mu_{\rm d} - 2\mu_{\rm s}), \\
\mu_{Y_c} &= \tfrac{1}{3}(\mu_{\rm u} + \mu_{\rm d} + \mu_{\rm s} - 3\mu_{\rm c}),
\end{aligned} \tag{A.2}$$

where the quantum number Y_c has been defined by $Y_c = (3/4)B - C$ with baryon number B and charmness number C. The relation (A.2) can be rewritten as

$$\begin{aligned}
\mu_{\rm u} &= \tfrac{1}{3}\mu_B + \tfrac{1}{2}\mu_I + \tfrac{1}{3}\mu_Y + \tfrac{1}{4}\mu_{Y_c}, \\
\mu_{\rm d} &= \tfrac{1}{3}\mu_B - \tfrac{1}{2}\mu_I + \tfrac{1}{3}\mu_Y + \tfrac{1}{4}\mu_{Y_c}, \\
\mu_{\rm s} &= \tfrac{1}{3}\mu_B - \tfrac{2}{3}\mu_Y + \tfrac{1}{4}\mu_{Y_c}, \\
\mu_{\rm c} &= \tfrac{1}{3}\mu_B - \tfrac{3}{4}\mu_{Y_c}.
\end{aligned} \tag{A.3}$$

This final form is also natural, since the coefficients on the right-hand side of Eq. (A.3) are that u, d, s, c quarks have the quantum numbers of own.

In Fig. A.4, we show the flavor diagonal and off-diagonal susceptibilities $\chi^{(2)}_{ff'}$ as a function of T in the 2+1+1 flavor system. For the 2+1 flavor sector, good agreement is seen between LQCD data and the HQC results, i.e., $\chi^{(2)}_{\rm uu}$, $\chi^{(2)}_{\rm ud}$, $\chi^{(2)}_{\rm ss}$, $\chi^{(2)}_{\rm us}$. On the other hand, $\chi^{(2)}_{\rm cc}$ and $\chi^{(2)}_{\rm uc}$ are not consistent with LQCD data, its directly relate to c quark. However, HQC model results is same order as LQCD data without c quark dependence of $f_{\rm H}$, i.e. $f^{(2)}_{\rm H,cf}(f = {\rm u, s, c})$. These supports the statement that c quark does not have a effect for the 2+1 flavor subsystem composed of u, d, s quarks.

Above all, the behavior of c quark is isolated from the dynamics among u, d, s quarks and makes no change the quark-hadron transition.

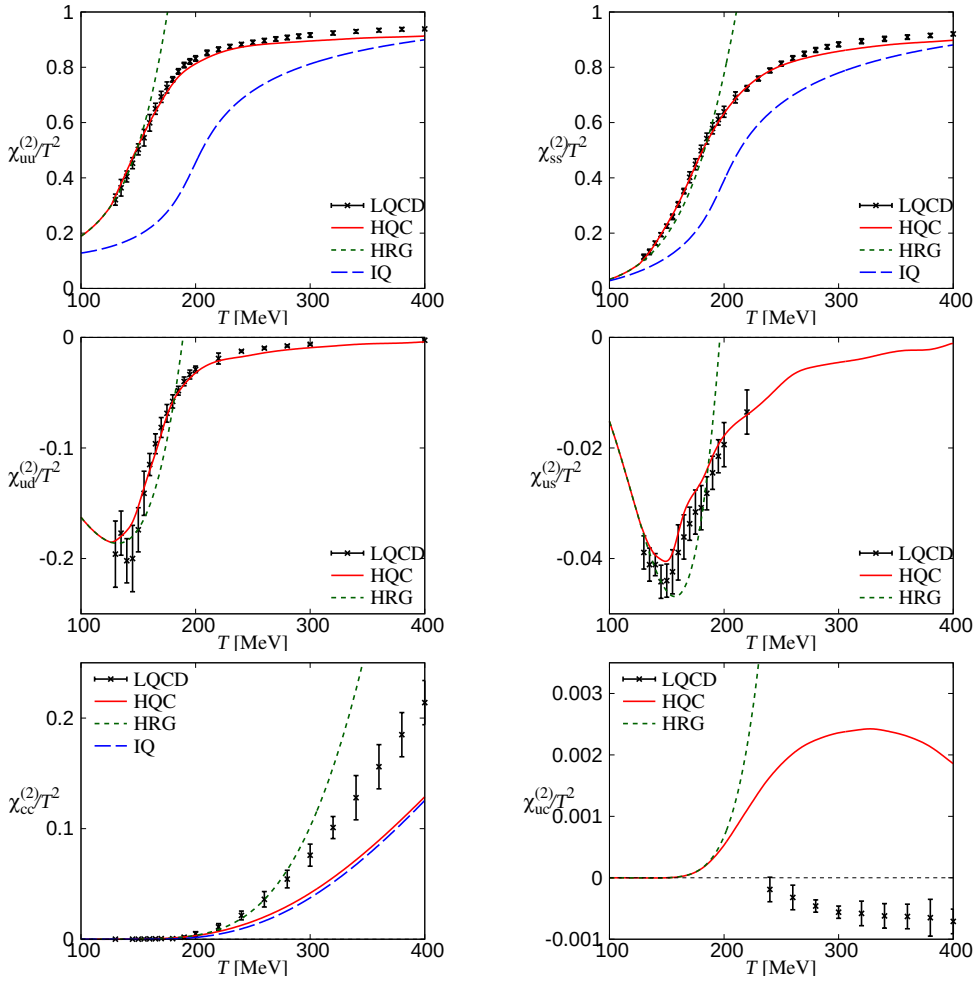

Fig. A.4: T dependence of flavor diagonal and off-diagonal susceptibilities, $\chi^{(2)}_{ff'}$, in the 2+1+1 flavor system with zero chemical potential. The solid line denotes the HQC result. The dotted line stands for the result of the HRG model, the dashed line corresponds to that of the IQ model. LQCD data (dots with error bars) are taken from Ref [23].

B A brief derivation of Polyakov potential

In Polyakov potential of this thesis,

$$\frac{\mathcal{U}(T,\Phi,\bar{\Phi})}{T^4} = -\frac{a(T)}{2}\Phi\bar{\Phi} + b(T)\log\{1 - 6\Phi\bar{\Phi} + 4(\Phi^3 + \bar{\Phi}^3) - 3(\Phi\bar{\Phi})^2\}, \tag{B.1}$$

parameters $a(T), b(T)$ are determined by reproducing pressure, entropy density and energy density of LQCD simulations [12].

On the other hand, the coefficients of $1 - 6\Phi\bar{\Phi} + 4(\Phi^3 + \bar{\Phi}^3) - 3(\Phi\bar{\Phi})^2$ in Eq. (B.1) are determined by Fadeev-Popov determinant of gluon-field measure [32, 33].

In this section, we show a brief derivation of $1-6\Phi\bar{\Phi}+4(\Phi^3+\bar{\Phi}^3)-3(\Phi\bar{\Phi})^2$. Using Wilson-loop matrix $\mathrm{SU}(3) \ni L(x) = P\exp\left[ig\int_0^{1/T} d\tau A_4(x)\right]$ with the temporal gauge field $A_4 = A_4^a(\lambda_a/2)$ (Gell-mann matrices $\lambda_a (a = 1 \sim 8)$), the partition function is described as

$$Z = \int DL \int DqD\bar{q}e^{-S_E}, \tag{B.2}$$

where q is quark field, S_E is a Euclidean action.

One can make always a diagonal matrix L_{diag} from L by finding a $b \in \mathrm{SU}(3)$ as $L = bL_{\mathrm{diag}}b^\dagger$. Then, we are able to write the L_{diag} as follow;

$$L_{\mathrm{diag}} = \begin{pmatrix} e^{i\phi_1} & & \\ & e^{i\phi_2} & \\ & & e^{i\phi_3} \end{pmatrix}, \tag{B.3}$$

where ϕ_1, ϕ_2, ϕ_3 are real parameters.

Using the parameters, the integration of L becomes

$$\begin{aligned} \int dL &= \int_0^{2\pi} \frac{d\phi_1}{2\pi}\frac{d\phi_2}{2\pi}\frac{d\phi_3}{2\pi} \prod_{j<k}^{3} |e^{-i\phi_j} - e^{-i\phi_k}|^2 \\ &= \int_0^{2\pi} \frac{d\phi_1}{2\pi}\frac{d\phi_2}{2\pi}\frac{d\phi_3}{2\pi} \prod_{j<k}^{3} 4\sin^2\left(\frac{\phi_j - \phi_k}{2}\right) \\ &\equiv \int_0^{2\pi} \frac{d\phi_1}{2\pi}\frac{d\phi_2}{2\pi}\frac{d\phi_3}{2\pi} \mathcal{M}(\phi_1, \phi_2, \phi_3). \end{aligned} \tag{B.4}$$

Furthermore, we rewrite the $\mathcal{M}$ with $\Phi = \langle (1/3)\mathrm{tr}_c L_{\mathrm{diag}}\rangle = (1/3)(e^{i\phi_1} + e^{i\phi_2} + e^{i\phi_3})$ and $\bar{\Phi} = \Phi^*$ as

$$\mathcal{M} = C(1 - 6\Phi\bar{\Phi} + 4(\Phi^3 + \bar{\Phi}^3) - 3(\Phi\bar{\Phi})^2), \tag{B.5}$$

where C is a constant overall factor.

Finally, the partition function becomes

$$Z = \int \frac{d\phi_1}{2\pi}\frac{d\phi_2}{2\pi}\frac{d\phi_3}{2\pi} \int DqD\bar{q}e^{-S_E + \log\mathcal{M}(\Phi,\bar{\Phi})}. \tag{B.6}$$

Hence, we obtain the Polyakov potential (B.1).

Bibliography

[1] L. D. McLerran and B. Svetitsky, Phys. Rev. D **24**, 450 (1981). doi:10.1103/PhysRevD.24.450

[2] P. de Forcrand and O. Philipsen, Nucl. Phys. B **642**, 290 (2002) doi:10.1016/S0550-3213(02)00626-0 [hep-lat/0205016].

[3] P. de Forcrand and O. Philipsen, Nucl. Phys. B **673**, 170 (2003) doi:10.1016/j.nuclphysb.2003.09.005 [hep-lat/0307020].

[4] Y. Aoki, G. Endrődi, Z. Fodor, S. D. Katz and K. K. Szabó, Nature **443**, 675 (2006).

[5] N. Cabibbo and G. Parisi, Phys. Lett. **59B**, 67 (1975). doi:10.1016/0370-2693(75)90158-6

[6] M. Albright, J. Kapusta and C. Young, Phys. Rev. C **90**, 024915 (2014) [arXiv:1404.7540 [nucl-th]].

[7] M. Asakawa, T. Hatsuda, Phys. Rev. B **55**, 7 (1997).

[8] R. Hagedorn, Lect. Notes Phys. **221**, 53 (1985). doi:10.1007/978-3-319-17545-4. 25

[9] P. Huovinen and P. Petreczky, Nucl. Phys. A **837**, 26 (2010) doi:10.1016/j.nuclphysa.2010.02.015 [arXiv:0912.2541 [hep-ph]].

[10] K. V. Olive *et al.* (Particle Data Group), Chin. Phys. C **38**, 090001 (2014).

[11] S. Borsányi, G. Endrődi, Z. Fodor, S. D. Katz, S. Krieg, C. Ratti, and K. K. Szabo, JHEP **08**, 053 (2012).

[12] S. Rößner, C. Ratti, and W. Weise, Phys. Rev. D **75**, 034007 (2007).

[13] S. Borsányi, Z. Fodor, C. Hoelbling, S. D. Katz, S. Krieg, C. Ratti, and K. K. Szabo, JHEP **09**, 073 (2010).

[14] S. Borsányi, Z. Fodor, S. D. Katz, S. Krieg, C. Ratti, and K. K. Szabo, JHEP **01**, 138 (2012).

[15] S. Borsanyi *et al.* [Wuppertal-Budapest Collaboration], JHEP **1009**, 073 (2010) doi:10.1007/JHEP09(2010)073 [arXiv:1005.3508 [hep-lat]].

[16] Y. Aoki, S. Borsányi, S. Dürr, Z. Fodor, S. D. Katz, S. Krieg, and K. K. Szabó, JHEP **06**, 088 (2009).

[17] M. Gell-Mann, R. Oakes, B. Renner, Phys. Rev. **175**, 2195 (1968).

[18] J. Jankowski, D. Blaschke and M. Spalinski, Phys. Rev. D **87**, no. 10, 105018 (2013) doi:10.1103/PhysRevD.87.105018 [arXiv:1212.5521 [hep-ph]].

[19] T. Hatsuda and S. H. Lee, Phys. Rev. C **46**, no. 1, R34 (1992). doi:10.1103/PhysRevC.46.R34

[20] T. Hatsuda, and S.H. Lee, Phys. Rev. C **46**, 34 (1992).

[21] K. Fukushima, Phys. Lett. B **591**, 277 (2004); Phys. Rev. D **77**, 114028 (2008).

[22] K. Kashiwa, H. Kouno, M. Matsuzaki, and M. Yahiro, Phys. Lett. B **662**, 26 (2008).

[23] S. Borsányi *et al.*, Nature **539**, 69 (2016) [arXiv:1606.07494 [hep-lat]].

[24] H. Kouno, T. Makiyama, T. Sasaki, Y. Sakai, and M. Yahiro, J. Phys. G: Nucl. Part. Phys. **40**, 095003 (2013).

[25] A. Miyahara, Y. Torigoe, H. Kouno and M. Yahiro, Phys. Rev. D **94**, 016003 (2016) [arXiv:1604.05002 [hep-ph]].

[26] M. Asakawa, T. Hatsuda, Phys. Rev. D **55**, 4488 (1997).

[27] L. Landau and E. Lifshitz, Statistical Physics (Pergamon, New York, 1980).

[28] R. Bellwied, S. Borsányi, Z. Fodor, S. D. Katz, A. Pasztor, C. Ratti and K. K. Szabo, Phys. Rev. D **92**, 114505 (2015) [arXiv:1507.04627 [hep-lat]].

[29] N. Haque, J. O. Andersen, M. G. Mustafa, M. Strickland and N. Su, Phys. Rev. D **89**, 061701 (2014) [arXiv:1309.3968 [hep-ph]]; N. Haque, A. Bandyopadhyay, J. O. Andersen, M. G. Mustafa, M. Strickland and N. Su, JHEP **1405**, 027 (2014) [arXiv:1402.6907 [hep-ph]].

[30] S. Borsányi, G. Endrodi, Z. Fodor, A. Jakovac, S. D. Katz and K. K. Szabo, JHEP **1007**, 056 (2012).

[31] S. Ejiri, Phys. Rev. D **77**, 014508 (2008) [arXiv:0706.3549 [hep-lat]].

[32] H. Reinhardt, Nucl. Phys. B **503**, 505 (1997) doi:10.1016/S0550-3213(97)00489-6 [hep-th/9702049].

[33] J. B. Kogut, M. Snow and M. Stone, Nucl. Phys. B **200**, 211 (1982). doi:10.1016/0550-3213(82)90065-7